RESEARCH ARTICLE | JUNE 01 2026

The role of charge distribution in the modeling of polyatomic ions: The nitrate anion case

Special Collection: Festschrift in honor of Christoph Dellago: Exploring Paths and Barriers in Statistical Mechanics

M. Cruz-Sánchez ; F. Gámez ; C. Vega ; V. M. Trejos

J. Chem. Phys. 164, 214503 (2026)
https://doi.org/10.1063/5.0329408

The Journal of Chemical Physics ARTICLE pubs.aip.org/aip/jcp

The role of charge distribution in the modeling of polyatomic ions: The nitrate anion case

Cite as: J. Chem. Phys. 164, 214503 (2026); doi: 10.1063/5.0329408
Submitted: 17 February 2026 • Accepted: 6 May 2026 •
Published Online: 1 June 2026

M. Cruz-Sánchez,[1] F. Gámez,[2] C. Vega,[2,a)] and V. M. Trejos[1,a)]

AFFILIATIONS

[1] Departamento de Química, Universidad Autónoma Metropolitana-Iztapalapa, Av. San Rafael Atlixco 186, Col. Vicentina, 09340 Ciudad de México, Mexico
[2] Departamento de Química Física, Universidad Complutense de Madrid, 28040 Madrid, Spain

Note: This paper is part of the Special Topic Festschrift in Honor of Christoph Dellago: Exploring Paths and Barriers in Statistical Mechanics.
[a)]**Authors to whom correspondence should be addressed:** cvega@quim.ucm.es and vtrejos@izt.uam.mx

ABSTRACT

Nitrate salts are widely used in agriculture, industrial chemistry, and food preservation. Using computer simulations based on the intermolecular parameters of the extended Madrid-2019 force field [V. M. Trejos *et al.*, J. Chem. Phys. **159**(22), 224501 (2023)], we examine the effect of intramolecular partial charge distributions of the nitrate anion on the temperature of maximum density (TMD) of aqueous $NaNO_3$, KNO_3, and NH_4NO_3 solutions. A specific internal charge distribution improves agreement with experimental TMD data relative to the original force field and enables predictions for systems lacking experimental measurements. Densities are largely insensitive to the charge distribution, while transport properties (diffusion coefficients and viscosities) show only minor variations. In contrast, structural properties are sensitive to the choice of the charge distribution. The original force field provides better agreement with neutron diffraction structural data than the model yielding the most accurate TMD. An intermediate charge distribution is therefore selected as a compromise, providing a balanced description of all properties. Empirical force fields cannot reproduce all properties simultaneously; however, an appropriate parameter selection, including the intramolecular charge distribution as an additional degree of freedom, yields a consistent description of thermodynamic, transport, and structural properties.

I. INTRODUCTION

From a commercial perspective, nitrate salts such as $NaNO_3$, KNO_3, and NH_4NO_3 are widely used in the chemical and pharmaceutical industries.[1,2] A major application of nitrate salts is their role as nitrogen sources in agriculture. For example, calcium nitrate and ammonium nitrate solutions are commonly employed to supply nitrogen directly to plants, thereby enhancing growth and improving soil productivity.[3] These solutions provide readily available nitrate nitrogen, which is particularly beneficial for rapid plant growth and in nutrient-poor soils. In addition to agricultural applications, sodium nitrate is used as an oxidizing and clarifying agent in glass production, where it helps remove bubbles and impurities. The nitrate ion also participates in redox processes, including its chemical reduction in aqueous solution, that is relevant in several industrial and environmental contexts.[4] Moreover, increased concentrations of nitrate and ammonium ions in acid rain have significantly affected precipitation pH, leading to important environmental consequences.[5] Water contamination by nitrate is another major global concern. Continuous monitoring of nitrate levels in groundwater and drinking water is essential to ensure water safety. Elevated nitrate concentrations can adversely affect human health and disrupt ecological systems. Therefore, the development of reliable detection and quantification methods for nitrate ions in aqueous environments remains a pressing need.[6]

Despite their widespread use and environmental relevance, the accurate calculation of thermodynamic, structural, and dynamic properties of aqueous nitrate salt solutions remains challenging. This difficulty arises primarily from the complex nature of electrostatic interactions between ions, as well as between ions and

water molecules. In this context, molecular simulations have become increasingly important in chemistry, biology, and biophysics.[7] In particular, computer simulations can complement experiments by providing detailed microscopic information that is often inaccessible experimentally. In many cases, the scarcity, limited accuracy, or inconsistency of experimental data (i.e., differing results reported by independent groups without clear consensus) further complicates reliable theoretical predictions. In this context, molecular simulation approaches based on well-constructed force fields provide a valuable and practical framework for describing nitrate salt solutions over a wide range of concentrations. Such molecular models also enable reliable extrapolations to temperature and pressure conditions for which experimental data are unavailable. Among these approaches, molecular dynamics (MD) simulations represent a powerful tool for studying aqueous nitrate solutions, particularly in regimes where experimental information is limited. However, the accuracy of MD simulations depends on the availability of suitable force fields.

Several models have been proposed to simulate the NO_3^- anion.[8,9] In recent years, the use of scaled charges for ions in water has demonstrated excellent accuracy in describing aqueous electrolyte solutions,[10–14] and this approach has been extended to nitrate ions as well.[15] The use of scaled charges effectively incorporates polarization effects and accounts for charge transfer between ions and surrounding water molecules in solution.[16–19] As a result, the use of scaled charges has been shown to provide a reliable description of many properties of aqueous electrolyte solutions.[20] It is worth noting, however, that different scaled charges may accurately reproduce certain properties while performing less satisfactorily for others.[12] For instance, while a scaled charge of $\pm 0.85e$ provides a good compromise for reproducing a wide range of thermodynamic and structural properties, the transport properties are often better described using lower scaled charges, such as $\pm 0.75e$.[12,21,22]

The motivation for the present work comes from our earlier work on the extension of the Madrid-2019 force field for the parametrization of nitrate and ammonium ions in aqueous solutions using the TIP4P/2005 water model (see Ref. 15). In that study, we proposed a force field capable of accurately predicting densities, ion–ion and ion–solvent structural properties, and transport properties for a wide range of nitrate salt solutions. The force field was tested for eight different nitrate salts and exhibited excellent performance. Notably, to the best of our knowledge, that work represented the first attempt to predict the concentration dependence of the density and transport properties of nitrate salt solutions at high concentrations using MD simulations with the TIP4P/2005 water model. At that time, the temperature of maximum density (TMD) was not investigated, primarily due to the absence of experimental TMD data for aqueous nitrate salt solutions in the literature. Consequently, the force field developed in Ref. 15 was not optimized with respect to this property. Later, some of the authors of the present work reported experimental measurements of the TMD at $1m$ and room pressure for several aqueous nitrate salt solutions. The corresponding TMD values were also computed using MD simulations with the force field proposed in Ref. 15. These results revealed an anomalously large deviation in the predicted TMD for $1m$ $NaNO_3$ solutions, amounting to ~6.3 K.[23] This deviation is larger than those typically observed for other electrolyte solutions modeled with the Madrid-2019 force field, for which deviations are usually on the order of 2–3 K for atomic ions.[12,24,25] This unexpected discrepancy between the MD results and the experimental TMD values motivated the present study. It is worth noting that the TIP4P/2005 water model reproduces the TMD of pure water almost exactly, indicating that the observed deviation arises exclusively from the force field used for the nitrate salts. For polyatomic ions, in contrast to monoatomic ions, there exists an additional degree of freedom beyond the choice of the global scaled charge: multiple partial charge distributions can yield the same net ionic charge. Typically, these partial charges are derived from quantum chemical calculations, as was the case in our previous force field.[15] However, the present results clearly indicate that this charge distribution fails to reproduce the experimental TMD of nitrate solutions. This observation raises the question of whether the intramolecular charge distribution itself plays a significant role in determining the TMD.

In this work, we explicitly address this question by exploring the effect of the intramolecular charge distribution on the TMD of aqueous nitrate solutions. We demonstrate that the charge distribution has a strong impact on the predicted TMD and propose several charge-distribution models that improve the agreement with the experimental data while preserving the overall accuracy for thermodynamic and dynamic properties. There are few studies analyzing how the internal charge distribution in polyatomic ions affects properties. Recently, Blazquez *et al.*[26] showed that, for the perchlorate anion (ClO_4^-), the internal charge distribution affects the TMD as well as other thermodynamic, structural, and dynamic properties. Similarly, de Lucas *et al.*[27] developed two force fields for the hydroxide ion (OH^-) with identical net charges but different partial charge distributions, observing noticeable differences in several properties. These findings highlight the importance of investigating the effects of intramolecular charge distribution of polyatomic ions, such as the planar nitrate ion (NO_3^-).

It is reasonable to anticipate that the impact of intramolecular charge distribution on the TMD will be more pronounced for planar ions such as NO_3^- than for tetrahedral ions such as ClO_4^-.[26] In the case of ClO_4^-, water molecules interact primarily with the oxygen atoms, whereas for NO_3^-, water molecules can interact with both nitrogen and oxygen atoms, leading to distinct solvation/coordination structures. The purpose of this work is, therefore, to develop a new force field for the nitrate ion by assigning a net scaled charge of $-0.85e$ while optimizing the intramolecular charge distribution to enhance the prediction of the TMD. We also demonstrate the strong impact of the intramolecular charge distribution on the predictions of the TMD for planar polyatomic ions. If the TMD of pure water is becoming a key target property in the development of water force fields over the past two decades, it is clear that it should also be considered a target property in the development of force fields for electrolyte solutions.

This paper is organized as follows. In Sec. II, we describe the intermolecular pair potential, the MD simulation details, the quantum chemistry calculations, and the theoretical framework used to compute dynamic properties such as self-diffusion coefficients and viscosities. In Sec. III, we examine the role of the intramolecular charge distribution on the TMD of aqueous NO_3^- solutions. We then present results for thermodynamic properties (TMDs, bulk densities), dynamic properties (self-diffusion coefficients and shear viscosities), and structural properties [radial distribution functions (RDFs)], obtained using an optimized nitrate nitrogen charge distribution. In Sec. IV, we present the results for the suggested force

field of the nitrate anion resulting from this work. Finally, Sec. V summarizes the main findings and provides concluding remarks.

II. MOLECULAR SIMULATIONS

A. Intermolecular pair potential

In this work, we consider a system composed of water and nitrate salts. The intermolecular interactions between atoms are described as the sum of a Lennard-Jones (LJ) contribution and an electrostatic term arising from Coulombic interactions. The pair potential, $u(r_{ij})$, between two atoms i and j in different molecules and separated by a distance r_{ij} is given by

$$u(r_{ij}) = 4\varepsilon_{ij}\left[\left(\frac{\sigma_{ij}}{r_{ij}}\right)^{12} - \left(\frac{\sigma_{ij}}{r_{ij}}\right)^{6}\right] + \frac{1}{4\pi\varepsilon_0}\frac{q_i q_j}{r_{ij}}, \tag{2.1}$$

where σ_{ij} and ε_{ij} are the LJ diameter and well depth, respectively; q_i and q_j are the partial charges of atoms i and j; and ε_0 is the vacuum permittivity. The nitrate anion (NO_3^-) and its corresponding counterions (i.e., Na^+, K^+, NH_4^+, Rb^+, Cs^+, Li^+, Ca^{2+}, and Mg^{2+}) were modeled using the extended Madrid-2019 force field,[15] which builds upon the original Madrid-2019 model.[11] This force field has been successfully applied to ionic systems in combination with the TIP4P/2005 water model, using a net scaled charge of $q_{\text{scaled}} = \pm 0.85e$. The LJ parameters ($\sigma_{ij}$ and ε_{ij}) and the Coulombic parameters (atomic charges, q_i) for the nitrate ion and its counterions are reported in Tables I and II of Ref. 15.

B. Molecular dynamics simulations

All molecular dynamics (MD) simulations were performed using the GROMACS simulation package (version 4.6.5).[28,29] Thermodynamic properties, such as densities and the TMD, as well as structural properties, including radial distribution functions (RDFs), were obtained from simulations carried out in the isothermal–isobaric (NpT) and canonical (NVT) ensembles. The simulated systems consisted of 555 water molecules and the corresponding numbers of nitrate ions and counterions required to achieve the target molalities. For example, a system containing 555 water molecules requires ten molecules of salt to represent a $1m$ solution, where m is the molality defined as the number of moles of salt per kilogram of water. Temperature and pressure were controlled using the Nosé–Hoover thermostat[30,31] and the Parrinello–Rahman barostat,[32] respectively, both with coupling time constants of 2 ps. The equations of motion were integrated using the leap-frog algorithm[33] with a time step of 2 fs. Periodic boundary conditions were applied in all three spatial xyz directions. As discussed in Sec. II A, the intermolecular pair potential consists of LJ and Coulombic contributions. A cutoff radius of 1.0 nm was employed for both van der Waals and short-range electrostatic interactions. Long-range corrections to the energy and pressure were applied to the LJ contribution, while long-range electrostatic interactions were treated using the smooth Particle Mesh Ewald (PME) method.[34] The LJ parameters and atomic charges for the nitrate anion (NO_3^-) and the corresponding counterions (monovalent ions Na^+, K^+, Cs^+, Li^+, Rb^+, and NH_4^+, and divalent ions Ca^{2+} and Mg^{2+}) were taken from the Madrid-2019 force field[11,35] and its recent extension for nitrate and ammonium ions.[15] It should be mentioned that we have recently extended the Madrid-2019 force field to the ferrous Fe^{2+} cation[36] so that the force field of this work could also be used to study aqueous solutions of ferrous nitrate [$Fe(NO_3)_2$]. Water molecules were modeled using the TIP4P/2005 model.[37] Geometrical constraints for nitrate salts were maintained using the LINear Constraint Solver (LINCS) algorithm,[29,38] while the Systematic Holonomic Algorithm for constraining bond lengths (SHAKE) algorithm[39] was applied to salts containing the ammonium ion. For the nitrogen atoms in both the ammonium and nitrate ions, the LJ size parameter was fixed to 3.15 Å. The nitrate ion (NO_3^-) was modeled as a planar molecule with an $\widehat{ONO}$ angle of 120° and an O_n–N_n bond length of 1.256 Å, where O_n and N_n are the oxygen and nitrogen atoms of the nitrate anion, respectively. For the ammonium ion (NH_4^+), the $\widehat{HNH}$ angle was set to 109.5°, and the N_a–H_a bond length to 1.010 Å, as reported in Ref. 15, where N_a and H_a denote the nitrogen and hydrogen atoms of the ammonium ion, respectively. The crossed LJ parameters (σ_{ij}, ε_{ij}) do not follow the Lorentz–Berthelot combination rules. All parameters are reported in Ref. 15, along with the corresponding topology file (topol.top) containing the original parametrization for the intramolecular charge distribution.

For simulations in the density–molality plane, production runs of ~50 ns (for each thermodynamic state) were performed, whereas simulations in the density–temperature plane were extended to ~200 ns (for each thermodynamic state) to accurately determine the TMD. For the determination of the TMD, a third-order polynomial fit to the MD data was employed. To illustrate and familiarize the reader with the concept of intramolecular charge distribution in the nitrate ion (NO_3^-), Table I summarizes the LJ parameters and partial charges of the model reported in Ref. 15, as well as those of the model that best reproduces the experimental TMD, hereafter referred to as Model 5. Both models use a net scaled charge of $q_{\text{scaled}} = \pm 0.85e$. In the original parametrization, the nitrate nitrogen charge is $q_N = 0.6749e$,[15] whereas in Model 5, the corresponding value is $q_N = -0.1000e$, which corresponds to the modified model that best reproduces the TMD.

TABLE I. Summary of the force field parameters for the Coulombic (atomic charges, q_i) and LJ (σ_{ii}, ε_{ii}) contributions to the pair potential for the nitrate anion (NO_3^-). The geometry of the NO_3^- is defined by an $\widehat{O_nN_nO_n}$ angle of 120° and an O_n–N_n bond length of 1.256 Å, where O_n and N_n are the oxygen and nitrogen atoms of the nitrate anion, respectively, as reported in Ref. 15. The LJ parameters σ_{ii} and ε_{ii} are presented in units of Å and kJ/mol, respectively, while the Coulombic charges are presented in electron units (e). In both models considered, the nitrate anion has a net charge of $\pm 0.85e$, in accordance with the Madrid-2019 force field. See Ref. 15 for a complete description of the LJ parameters and for a GROMACS topology file.

NO_3^-	σ_{ii} (Å)	ε_{ii} (kJ/mol)	q_i (e)
Original parametrization from Ref. 15			
N_n	3.1500	0.7110	0.6749
O_n	2.8600	0.8786	−0.5083
Modified parametrization			
N_n	3.1500	0.7110	−0.1000
O_n	2.8600	0.8786	−0.2500

C. Quantum chemistry calculations

To obtain the intramolecular quantum charge distribution of the nitrate ion (NO_3^-), quantum chemistry calculations were performed based on geometry optimizations using the *Gaussian* software package.[40] Density Functional Theory (DFT) calculations were carried out at the B3LYP/6-311++G(d,p) level of theory. The resulting wavefunction file was subsequently used as input for the *Multiwfn* program,[41] where atomic charges were evaluated using several methods. When using the Atomic Dipole Moment Corrected Hirshfeld (ADCH) charge analysis approach, the quantum-derived partial charges for the nitrate ion were found to be $q_N = 0.5577$ for the nitrogen atom and $q_O = -0.5192e$ for each oxygen atom. Since the Madrid-2019 force field uses a net scaled charge of $\pm 0.85e$, the corresponding scaled charges used in our MD simulations are $q_N = 0.4740e$ and $q_O = -0.4414e$ for the nitrogen and oxygen atoms, respectively. These values provide a reliable reference for the intramolecular electronic charge distribution of the nitrate ion from a quantum-mechanical perspective and serve as a physically meaningful baseline for the force-field parametrization explored in this work.

It is worth noting that in our previous force field,[15] a nitrogen charge of $q_N = 0.6749e$ was used.[23] This atomic charge was taken from Refs. 8, 42, and 43 for the NO_3^- ion and subsequently scaled to yield a global charge of $\pm 0.85e$. Specifically, the original value of $q_N = 0.7940e$ was rescaled to $q_N = 0.6749e$ in Model 1.[15] This example illustrates how different quantum chemical calculations can lead to different partial charges for the nitrate nitrogen atom (e.g., $0.7940e$ vs $0.5577e$). When scaled to a total charge of $\pm 0.85e$, these values result in nitrogen charges of $0.6749e$ and $0.4740e$, respectively. As will be shown below, neither of these two values of the charge provides a satisfactory description of the TMD of aqueous nitrate salt solutions.

It must be emphasized that, in classical non-polarizable force fields, the assignment of atomic partial charges remains one of the main sources of uncertainty, since these quantities are not direct quantum mechanical observables and depend strongly on the chosen partitioning scheme. Different methodologies (e.g., Hirshfeld, CM5, RESP, MK, VDD, and MBIS) can yield significantly different charge distributions even when based on the same underlying electronic density, leading to a wide spread of physically reasonable parametrizations (see Table II). Several strategies have been proposed to mitigate this ambiguity. A widely used approach is the scaling of charges derived from electronic structure calculations to effectively account for polarization effects in condensed phases.[44] This procedure has been shown to improve the description of thermodynamic and transport properties, although the optimal scaling factor may depend on the property of interest. Alternatively, more recent methods aim to constrain the charge distribution using physically motivated quantities such as the molecular dipole moment or dielectric properties of the fluid, providing a more consistent link between microscopic charge assignment and macroscopic observables.[45]

Despite these advances, there is currently no consensus on a universally optimal charge derivation scheme for condensed-phase simulations. In practice, different approaches present distinct advantages and limitations. For instance, Hirshfeld-based methods tend to yield smaller and more transferable charges but often require empirical scaling, while electrostatic potential–based methods (e.g., RESP, MK) can better reproduce molecular electrostatics but may lead to overpolarized descriptions in condensed phases.

In this context, our approach follows a pragmatic strategy: rather than relying on a single charge derivation method, we systematically explore different charge distributions and assess their impact on experimentally accessible properties. This allows us to identify charge distributions that provide an optimal balance between thermodynamic, structural, and dynamic accuracy, while remaining consistent with quantum chemical trends.

D. Dynamic properties

1. Self-diffusion coefficients

The self-diffusion coefficient of each species (D_i) was obtained from the mean square displacement (MSD) of the particles using the Einstein relation, given by

$$D_i = \lim_{t\to\infty} \frac{1}{6t} \left\langle [\mathbf{r}_i(t) - \mathbf{r}_i(0)]^2 \right\rangle, \tag{2.2}$$

where $\mathbf{r}_i(t)$ and $\mathbf{r}_i(0)$ are the positions of the i-*th* particle at time t and at a reference time origin, respectively, and $\langle \cdots \rangle$ denotes the ensemble average of the MSD. The diffusion coefficients were determined from the linear regime of the MSD as a function of time, avoiding the initial subdiffusive regime. To account for

TABLE II. Partial charge distributions for the nitrate ion (NO_3^-) obtained from quantum chemistry calculations using different charge derivation methods. The table reports the atomic charges on nitrogen and oxygen (q_N, q_O), as well as the corresponding scaled values ($q_N \times 0.85$, $q_O \times 0.85$).

Method	$q_N(e)$	$q_O(e)$	$q_N(e)\times 0.85$	$q_O(e)\times 0.85$	References
ADCH	0.5577	−0.5192	0.4740	−0.4414	46
MBIS	0.9694	−0.6564	0.8239	−0.5579	47
Hirshfeld	0.2265	−0.4088	0.1925	−0.3475	48
CM5	0.0951	−0.3650	0.0808	−0.3103	48
VDD	0.3177	−0.4397	0.2700	−0.3737	49
RESP	1.0030	−0.6676	0.8526	−0.5675	50
MK	1.0053	−0.6683	0.8545	−0.5681	51

finite-size effects, all diffusion coefficients were corrected using the hydrodynamic correction proposed by Yeh and Hummer,[52]

$$D_{\mathrm{corr}} = D + 2.837\frac{k_B T}{6\pi\eta L}, \tag{2.3}$$

where D_{corr} is the corrected diffusion coefficient, D is the uncorrected value obtained from the MD simulations, T is the temperature, k_B is the Boltzmann constant, η is the simulated viscosity at the corresponding concentration, and L is the length of the simulation box.

2. Shear viscosity

The shear viscosity was computed following the methodology proposed by González and Abascal[53] for rigid molecular models, using the time autocorrelation functions of the five independent components of the pressure tensor, $[P_{\alpha\beta}(t)]$, within the Green–Kubo formalism,

$$\eta = \frac{V}{k_B T}\int_0^\infty \langle P_{\alpha\beta}(t)\, P_{\alpha\beta}(0)\rangle\, dt, \tag{2.4}$$

where V is the system volume. The methodology of González and Abascal[53] consists of first performing NpT simulations of 50 ns to obtain the average equilibrium volume V for each aqueous nitrate salt solution at the desired molality. Subsequently, NVT simulations of 50 ns were carried out using this average volume, during which the pressure tensor components $P_{\alpha\beta}(t)$ were saved on disk every 2 fs. The shear viscosity was then calculated from the time integral of the corresponding pressure autocorrelation functions using the Green–Kubo approach. All calculations of shear viscosities and self-diffusion coefficients were performed using larger systems containing 4440 water molecules and the corresponding ions and counterions in order to reduce finite-size effects and improve statistical accuracy.

III. RESULTS

As mentioned in the Introduction, we developed a set of different force fields for the nitrate ion (NO_3^-) by modifying its intramolecular charge distribution. In all models, the LJ parameters and the net scaled charge of the nitrate group and of monovalent cations were kept identical ($q_{\mathrm{scaled}} = \pm 0.85e$), allowing us to isolate the effect of the nitrate intramolecular charge distribution on the predicted thermodynamic, structural, and dynamic properties of aqueous solutions of planar molecular ions, such as nitrate salts. The only difference among the models lies in the value of q_{N} that modifies the partial charges assigned to the oxygen atoms within the nitrate ion (i.e., all models of this work use the LJ parameters that were proposed in our previous work[15]). Table III summarizes the six force-field variants proposed in this work, all of which differ exclusively in the value of q_{N}. The explored range spans from $q_{\mathrm{N}} = 0.6749e$ to $q_{\mathrm{N}} = -0.2125e$, thereby covering a wide range of charge distributions on the nitrogen atom.

In addition to the intramolecular charge distributions of the six force fields, we report in Table IV a summary of the quadrupole moments corresponding to the different charge distributions considered for the nitrate ion, including those obtained using the ADCH and MBIS methods. According to the IUPAC definition, the quadrupole moment tensor is given by

$$Q_{\alpha\beta} = \frac{1}{2}\sum_i q_i\left(3r_{i,\alpha}r_{i,\beta} - r_i^2\delta_{\alpha\beta}\right), \tag{3.1}$$

where q_i is the charge of particle i, $r_{i,\alpha}$ and $r_{i,\beta}$ are the Cartesian components $(\alpha, \beta \in x, y, z)$ of the position vector of atom i with respect to the chosen origin, r_i^2 is the squared distance of atom i from the origin, and $\delta_{\alpha\beta}$ is the Kronecker delta.

As shown in Table IV, Model 1 (when renormalized to the formal charge of the anion) exhibits a quadrupole moment of $Q_{xx} = -3.40$ D · Å, which is close to the value of $Q_{xx} = -3.84$ D · Å reported in Ref. 54 from MP2 *ab initio* calculations. However, it is important to note that these *ab initio* values correspond to an isolated nitrate anion in the gas phase, whereas in aqueous solution, the electronic density cloud of the ion of the ion is strongly modified by solvation and many-body polarization effects. As a result, the

TABLE III. Summary of the proposed intramolecular charge distributions for the nitrate ion (NO_3^-). All models share the same LJ parameters and a net scaled charge of $q_{\mathrm{scaled}} = \pm 0.85e$; only the partial charges assigned to the nitrogen and oxygen atoms are changed.

Model	$q_{\mathrm{N}}(e)$	$q_{\mathrm{O}}(e)$	Source
1	0.6749	−0.5083	Reference 15
2	0.3700	−0.4067	This work
3	0.1700	−0.3400	This work
4	0.0000	−0.2833	This work
5	−0.1000	−0.2500	This work
6	−0.2125	−0.2125	This work

TABLE IV. Values of the component Q_{xx} of the quadrupolar traceless tensor of the nitrate ion NO_3^- (with the origin of coordinates on the N atom, locating the *z*-axis perpendicular to the plane of the anion and taking into account that for the D_{3h} symmetry of the nitrate anion $Q_{yy} = Q_{xx}$). Values are reported for several charge distributions. The value obtained from *ab initio* calculations at the MP2 level using the CEP basis set, as reported in Ref. 54, is presented in the last row. For Models 1–6, which have a net anionic charge of −0.85*e*, we report the true value of $Q_{xx}(0.85e)$ in the fourth column, as well as the corresponding values that would be obtained for a unit charge, $Q_{xx}(e)$ (i.e., assuming a net charge of −1*e*), which are obtained by simply dividing the values in the fourth column by 0.85. For ADCH and MBIS charges, this renormalization is not needed, as the net charge of the anion is −1*e*.

Model	$q_{\mathrm{N}}(e)$	$q_{\mathrm{O}}(e)$	Q_{xx}(D · Å) ($q = -0.85e$)	Q_{xx}(D · Å) ($q = -1e$)
1	0.6749	−0.5083	−2.89	−3.40
2	0.3700	−0.4067	−2.31	−2.72
3	0.1700	−0.3400	−1.93	−2.27
4	0.0000	−0.2833	−1.61	−1.89
5	−0.1000	−0.2500	−1.42	−1.67
6	−0.2125	−0.2125	−1.21	−1.42
ADCH	0.5577	−0.5192		−2.95
MBIS	0.9694	−0.6564		−3.73
MP2 Ref. 54				−3.84

quadrupole moment of the nitrate ion in the liquid phase may differ significantly from its gas-phase counterpart.

The quadrupole moment provides physically meaningful information, as different intramolecular charge distributions with identical net charge map onto distinct multipolar representations of the ion. These differences directly affect the spatial distribution of the electrostatic potential and, consequently, the interaction of the nitrate ion with surrounding water molecules. Nevertheless, the good agreement of Model 1 with the gas-phase quadrupole does not necessarily imply a more accurate description of thermodynamic, structural, or dynamic properties in solution. In fact, as shown below, models that deviate significantly from the *ab initio* quadrupole (e.g., Models 5 and 6) yield a substantially improved description of the TMD, highlighting the limitations of directly transferring gas-phase electrostatic properties into condensed-phase force fields. A similar situation is observed for water. The dipole moment of an isolated water molecule is ~1.85 D, while in the liquid phase, it increases to about 2.7 D.[55–62] In contrast, widely used non-polarizable water models employ effective dipole moments in the range of 2.2–2.4 D,[63,64] which do not correspond exactly to either the gas-phase or liquid-phase values, but instead provide an optimal compromise for reproducing macroscopic properties.

These observations illustrate that quantum chemical electrostatic moments should be regarded as a useful reference, but not as strict targets for parametrization. Ultimately, the quality of a force field must be assessed based on its ability to reproduce a consistent set of experimental thermodynamic and structural properties, rather than on its agreement with gas-phase multipole moments alone.

A. Temperature of maximum density (TMD) and density at the TMD

Figure 1 shows the density as a function of temperature for aqueous $NaNO_3$ solutions at a concentration of 1*m* and room pressure, obtained using the six intramolecular charge distributions listed in Table III. In addition to the original charge distribution proposed in Ref. 15 (Model 1), we propose five additional charge-distribution models. The first three models are close to the original parametrization, while the remaining ones explore more substantial changes in the nitrate intramolecular charge distribution. As shown in Fig. 1(a), all models reproduce the overall temperature dependence of the solution density well. However, noticeable differences are observed in the prediction of the temperature of maximum density (TMD). For instance, deviations of 6.3 and 4.2 K with respect to the experimental TMD are obtained for Model 1 (original model[15]) and Model 3, respectively. Importantly, the deviation from the experimental TMD can be reduced by ~2 K compared to the value previously reported in Ref. 15. In Fig. 1(b), three additional models are analyzed, motivated by assigning a neutral charge to the nitrate nitrogen atom (Model 4) or a more negative charge (Model 6). In these cases, the predicted TMD values show significantly improved agreement with experimental data, highlighting the sensitivity of the TMD to the intramolecular charge distribution of the nitrate ion. Specifically, deviations of 3.0 and 2.2 K with respect to the experimental TMD are obtained for Models 4 and 6, respectively, representing a substantial reduction compared to the original parametrization of Model 1, which yields a deviation of 6.3 K for $NaNO_3$.[23] Consequently, Models 5 and 6 reproduce the experimental TMD of the $NaNO_3$ aqueous solution at a concentration of 1*m* with significantly improved agreement.

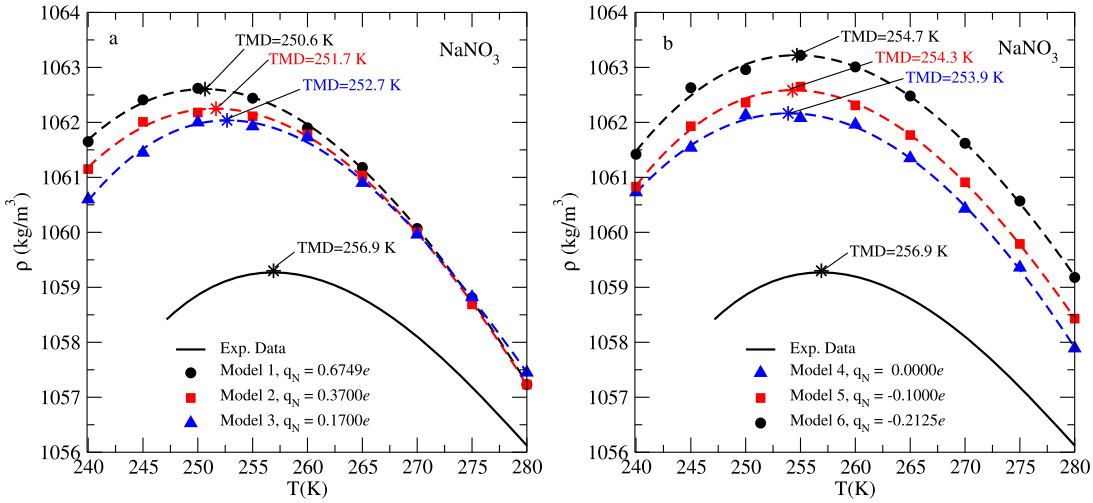

FIG. 1. Density as a function of temperature for aqueous $NaNO_3$ solutions at a concentration of 1*m* and room pressure, for different values of q_N in the pair potential of the nitrate ion (NO_3^-). Panel (a): q_N = 0.6749*e*,[15] 0.3700*e*, and 0.1700*e*; panel (b): q_N = −0.2125*e*, −0.1000*e*, and 0.0000*e*. MD results are shown as filled symbols and dashed lines, while continuous lines represent experimental data taken from Ref. 23. In both experimental and simulation results, the TMD is shown by stars. For all simulations, dashed lines correspond to third-order polynomial fits to the MD data. The MD simulations were performed using a net scaled charge of q_{scaled} = ±0.85*e* for both the nitrate anion and the Na^+ cation.[15]

Once the TMD of $NaNO_3$ has been calculated using six different values of q_N, it is of interest to further analyze the behavior of the TMD by considering two additional values of q_N charges, namely $q_N = 0.474\,04e$ (the partial charge obtained in this work from the ADCH method, as described in Sec. II C), and a large positive value, $q_N = 1e$. Figure 2 shows the TMD and the corresponding density at the maximum as functions of q_N for aqueous $NaNO_3$ solutions at $1m$ for all the models considered in this work. As shown in Fig. 2(a), the TMD exhibits a minimum near the original nitrate nitrogen charge, $q_N = 0.6749e$.[15] As q_N decreases, the TMD increases and gradually approaches the experimental TMD value. It is worth noting that, although the quantum-derived ADCH charge distribution ($q_N = 0.474\,04e$) slightly improves the TMD prediction relative to Model 1, the improvement is modest, from 250.65 to 251.06 K. This corresponds to a shift of only about 0.4–0.5 K compared to the experimental TMD value (256.9 K). Overall, decreasing the partial charge on the nitrogen atom relative to the value obtained in our original force field (Model 1) leads to improved agreement with experimental data, with the most accurate TMD predictions obtained when q_N adopts negative values. Finally, we have also estimated the TMD for the charge distribution obtained from the quantum MBIS approach[47] (scaled to a net charge of $0.85e$ for the ion) as it has been suggested to be a good method for parameterizing classical non-polarizable force fields. As shown in Table II, the nitrogen charge obtained for the nitrate ion using this method (when scaled to 0.85) is $q_N = 0.8239e$. According to Fig. 2(a), for this model, the TMD is ~250.9 K, which is very close to the value obtained using the quantum-derived charge distribution from the ADCH method ($q_N = 0.474\,04e$) but still 6 K below the experimental value.

Figure 2(b) presents the density at the TMD as a function of q_N. As q_N increases, the value of the density at the maximum density exhibits mild oscillations, while the deviation from the experimental density remains similar across all models. This indicates that the value of the density at the maximum density is significantly less sensitive to variations in the q_N than the TMD itself. Finally, for completeness, we include in Fig. 2 two additional MD simulation points obtained using a reduced scaled charge, $q_{scaled} = \pm 0.80e$. For these models, all the LJ parameters were kept identical to those of the force field with $q_{scaled} = \pm 0.85e$ (except the value of σ for the Na^+–O_w interaction, where we used the value optimized for $q_{scaled} = \pm 0.80e$ from our previous work[12]). Although a dedicated reparameterization for the nitrate group would likely be required to accurately describe densities at high concentrations for $q_{scaled} = \pm 0.80e$, our purpose here is illustrative. Notably, the model with $q_{scaled} = \pm 0.80e$ reproduces both the experimental TMD and density more accurately across the entire range of q_N values for $NaNO_3$. These results suggest that a reduced scaled charge ($q_{scaled} = \pm 0.80e$) could provide an improved description of the TMD for nitrates when compared to the commonly used value of $\pm 0.85e$.

It is worth noting that the ADCH quantum-derived charge distribution ($q_N = 0.474\,04e$) provides a useful initial estimate of how the electronic charge is distributed within the nitrate ion from the quantum-mechanics perspective. However, although extracting atomic charge information from quantum calculations is very useful for the development of force fields for polyatomic ions, it should be mentioned that different methods yield different values. Moreover, since partial charges are not observable quantities, the models obtained in this way should be tested with respect to their ability to reproduce thermodynamic, structural, and dynamic properties. In this context, the conclusion from the present work is clear. Using a water model that accurately reproduces the TMD of pure water and using the partial charge on the N atom obtained from quantum chemistry calculations made it impossible to reproduce the shift in the TMD for nitrate salts. From our perspective, the TMD is an experimentally observable property, and a properly designed force field should reproduce it as closely as possible to the experimental

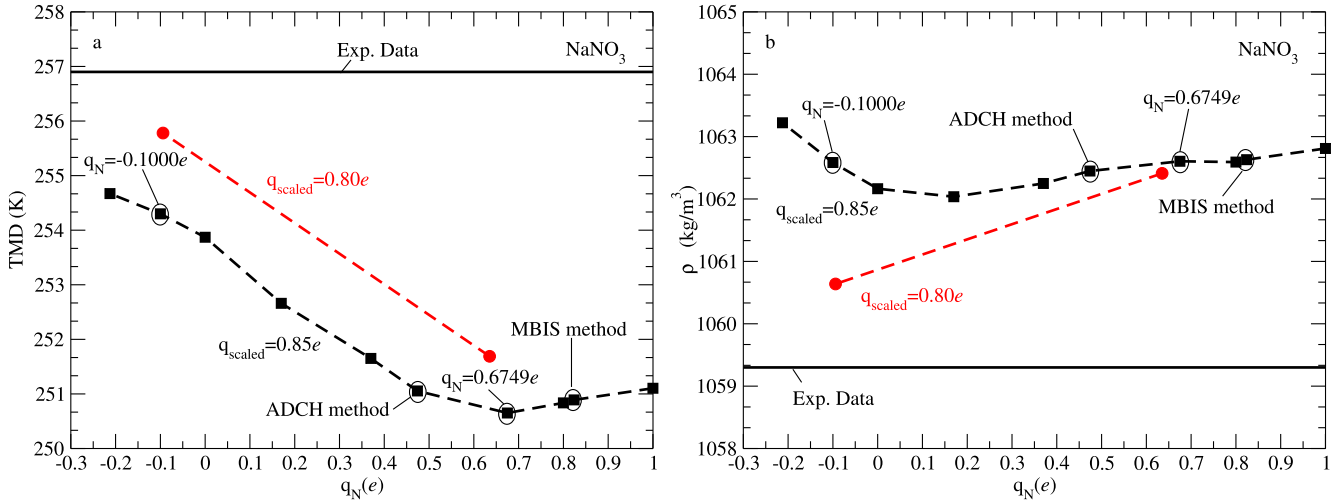

FIG. 2. Panel (a): The TMD as a function of q_N in the pair potential of the nitrate ion (NO_3^-) for aqueous $NaNO_3$ solutions at $1m$ and room pressure. Panel (b): The same as in panel (a), but for the corresponding density at the TMD. The MD results are shown as filled symbols, while dashed lines are included as guides to the eye. MD simulations were performed using two scaled charge values for both the nitrate anion and the Na^+ cation, $q_{scaled} = \pm 0.85e$ and $\pm 0.80e$.

results while maintaining accuracy in the structural properties. Accordingly, we argue that the intramolecular charge distribution can be treated as an additional degree of freedom in MD simulations that allows the improvement of properties without compromising the physical meaning of the charges within the molecule. However, selecting a force field using just one property does not seem to be a good strategy. It seems more reasonable to compute several properties before selecting the "best" model. We therefore perform an extended comparison between Model 1, our original force field, and Model 5, which provides a significantly improved prediction of the TMD of $NaNO_3$ solutions. Model 6 is not considered in this comparison, as assigning identical negative charges to both nitrogen and oxygen represents an extreme and physically less justified scenario. A first relevant test is to analyze the behavior of the TMD for other nitrate salts, since the previous discussion focused exclusively on $NaNO_3$.

Figure 3 shows the density as a function of temperature for aqueous salt solutions at a concentration of 1*m* and room pressure for three different salts. In panel (a), the TMD prediction for $NaNO_3$ is shown. A positive shift in the TMD of ~4 K (relative to Model 1) is observed, leading to significantly improved agreement with experimental data. In addition, Model 5 provides more accurate density predictions at temperatures below the TMD. In contrast, at temperatures above the TMD, a crossover behavior is observed, with Model 1 being slightly closer to the experimental density than Model 5, by ~0.1%. Panel (b) shows the corresponding results for KNO_3, showing an improvement of about 3.5 K in the location of the TMD. Finally, panel (c) presents the results for the more complex salt NH_4NO_3. In this case, Model 5 exhibits a remarkable agreement with experimental data for both the TMD and the corresponding density predicted with errors below 1%. Overall, an improvement of up to 4 K in the predicted TMD represents a significant step forward. All results obtained with Models 1 and 5 and shown in Fig. 3 are summarized in Table V. An important conclusion from these calculations is that modifying the charge distribution from Model 1 to Model 5 consistently improves the TMD

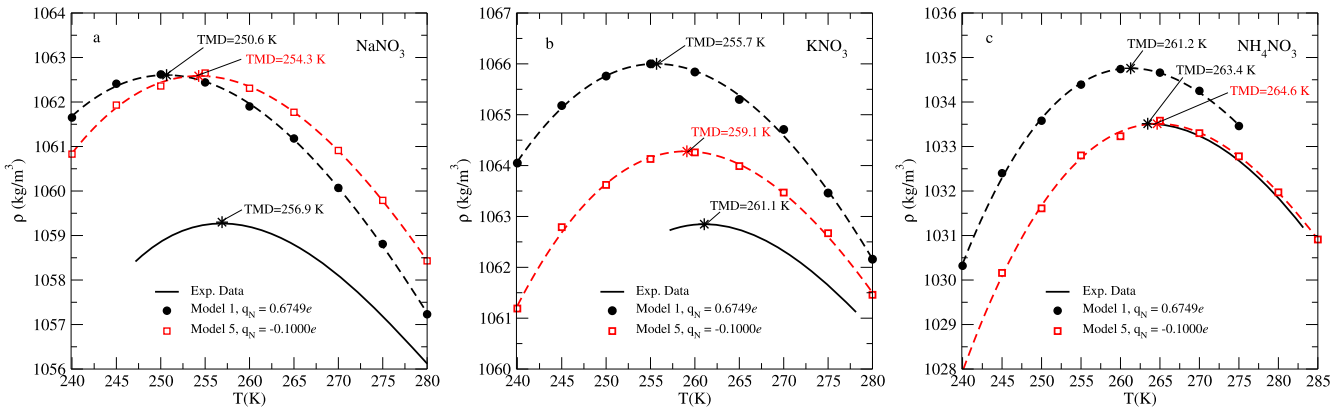

FIG. 3. Comparison between Models 1 and 5 for the density as a function of temperature in aqueous salt solutions at a concentration of 1*m* and room pressure. Panel (a): $NaNO_3$; panel (b): KNO_3; and panel (c): NH_4NO_3. MD results are shown as symbols and dashed lines, while continuous lines represent experimental data taken from Ref. 23. In both experimental and simulation results, the TMD is shown by stars. For all simulations, dashed lines correspond to third-order polynomial fits to the MD data. The MD simulations were performed using a net scaled charge of $q_{scaled} = \pm 0.85e$ for both the nitrate anion and the Na^+ cation.[15]

TABLE V. Comparison between Models 1, 3, and 5 for the TMD and the density at the TMD (ρ_{max}) of aqueous salt solutions at a concentration of 1*m* and room pressure. The systems considered are $NaNO_3$, KNO_3, and NH_4NO_3. Experimental data were taken from Ref. 23. The quantities *dev.* and *dev.*(%) denote the absolute deviation between experimental and simulated values and the corresponding relative percentage deviation, respectively, defined for TMD as $dev.(\%) = 100|TMD^{exp} - TMD^{sim}|/TMD^{exp}$. Uncertainties of the TMD from simulation are about 0.5 K.

Salt	Model	TMD^{sim} (K)	TMD^{exp} (K)	*dev.*	*dev.*(%)	ρ^{sim} (kg/m^3)	ρ^{exp} (kg/m^3)	*dev.*	*dev.*(%)
$NaNO_3$	1	250.60	256.90	6.3	2.5	1062.6	1059.3	3.3	0.3
	3	252.70	256.90	4.2	1.6	1062.0	1059.3	2.7	0.2
	5	254.30	256.90	2.6	1.0	1062.6	1059.3	3.3	0.3
KNO_3	1	255.70	261.10	5.4	2.1	1066.0	1062.8	3.2	0.3
	3	257.80	261.10	3.3	1.3	1065.3	1062.8	2.5	0.2
	5	259.10	261.10	2.0	0.8	1064.3	1062.8	1.5	0.1
NH_4NO_3	1	261.20	263.40	2.2	0.8	1034.8	1033.5	1.3	0.1
	3	263.90	263.40	0.5	0.2	1034.4	1033.5	0.9	0.1
	5	264.60	263.40	1.2	0.5	1033.5	1033.5	0.0	0.0

predictions for $NaNO_3$, KNO_3, and NH_4NO_3 with respect to experimental data.

As Model 5 significantly improves the prediction of the TMD compared to Model 1, it seems of interest to use this model to estimate the TMD of salts for which no experimental or simulation data have been reported in the literature before. Accordingly, Fig. 4 shows the density as a function of temperature for aqueous nitrate salt solutions at a concentration of 1*m*. Panel (a) presents the results for the monovalent salts $CsNO_3$, $RbNO_3$, and $LiNO_3$, while panel (b) shows the corresponding MD results for the divalent salts $Mg(NO_3)_2$ and $Ca(NO_3)_2$. For aqueous solutions, the lowering of the TMD of water, denoted as Δ, is defined as

$$\Delta = \mathrm{TMD}_{\mathrm{solution}} - \mathrm{TMD}_{\mathrm{water}}, \tag{3.2}$$

where the subscripts refer to the TMD of the aqueous solution and of pure water, respectively. For dilute aqueous solutions, this quantity follows the Despretz law,[65,66] which states that Δ varies linearly with the molality m according to

$$\Delta = K_m m, \tag{3.3}$$

where m is the molality of the solution and K_m is the Despretz constant, expressed in units of K kg mol^{-1}. The Despretz law can be interpreted within a group-contribution framework, in which each ion contributes independently to the macroscopic property. Accordingly, the Despretz constant of a salt can be decomposed into the individual ionic contributions $(K_m^{\pm})$[24] as follows:

$$K_m = (\nu_+ K_m^+ + \nu_- K_m^-), \tag{3.4}$$

where ν_+ and ν_- are the stoichiometric coefficients of the cation and anion, respectively. For example, in the case of $NaNO_3$, the salt dissociates into Na^+ ($\nu_+ = 1$, $K_m^+ = -11.6$ K kg mol^{-1}[24]) and NO_3^- ($\nu_- = 1$, $K_m^- = -11.4$ K kg as obtained from the results of this work for Model 5), yielding a total Despretz constant of $K_m = -23$ K kg mol^{-1} (Model 5). For the particular case of $LiNO_3$ at 1*m*, shown in Fig. 4(a), the TMD can be estimated using Eq. (3.4). Decomposing the salt into Li^+ ($\nu_+ = 1$, $K_m^+ = -3.0$ K kg mol^{-1}[24]) and NO_3^- ($\nu_- = 1$, $K_m^- = -11.4$ K kg mol^{-1}[23]) yields $K_m = -14.4$ K kg mol^{-1}. Using the TMD of pure water predicted by the TIP4P/2005 model, $\mathrm{TMD}_{\mathrm{water}} = 277.3$ K,[24] the estimated TMD for $LiNO_3$ at 1*m* is $\mathrm{TMD}_{\mathrm{LiNO_3}} = 262.9$ K. The MD simulations yield a value of TMD = 263.6 K [see Fig. 4(a)], which is in reasonably good agreement with the estimate based on the Despretz law. Applying the same procedure, the estimated TMDs for $Mg(NO_3)_2$ and $Ca(NO_3)_2$ are obtained by considering Mg^{2+} ($\nu_+ = 1$, $K_m^+ = -8.3$ K kg mol^{-1}[24]) and Ca^{2+} ($\nu_+ = 1$, $K_m^+ = -17.6$ K kg mol^{-1}[24]), respectively, together with two nitrate anions. This yields $\mathrm{TMD}_{\mathrm{Mg(NO_3)_2}} = 246.2$ K compared to the MD result $\mathrm{TMD}_{\mathrm{Mg(NO_3)_2}} = 251.7$ K for the 1*m* solution of $Mg(NO_3)_2$) and $\mathrm{TMD}_{\mathrm{Ca(NO_3)_2}} = 257.1$ K compared to the MD result $\mathrm{TMD}_{\mathrm{Ca(NO_3)_2}} = 258.9$ K for the 0.5*m* $Ca(NO_3)_2$ solution. The agreement obtained from the estimate of the Despretz law and from simulations is quite good (notice that the Despretz constant for the cations is the same as that reported in previous work, as the use of Model 5 instead of Model 1 only affects the value of the Despretz constant of the nitrate group). In fact, the Despretz constant obtained in this work for nitrate in Model 5 is −11.4, whereas the Despretz constant of Model 1 for the nitrate was reported to be −15.1. Since the Despretz constant for Model 1 is too large (in absolute value), the predictions of Model 1 for the TMD of divalent cations (i.e., Mg^{2+} or Ca^{2+}) are expected to deviate significantly from experimental values, when available.

B. Bulk densities

In Fig. 5, we present a comparison between Models 1 and 5 for the prediction of the density as a function of molality for aqueous nitrate salt solutions at 298.15 K and 1 bar. In panel (a), we show the density predictions for three salts, $NaNO_3$, KNO_3, and NH_4NO_3, over a range of molalities up to the solubility limit of each salt, which are 10.7, 3.8, and 12 mol/kg, respectively. In all cases, Model 5 reproduces the experimental densities with essentially the same level of accuracy and deviations as Model 1.[15] Notably, for these salts, the predictions obtained with Model 5 show excellent agreement with experimental data, indicating that the modification of the intramolecular charge distribution does not affect the density as long as the total charge and the LJ parameters remain unchanged. For completeness, we have also included additional density simulation points obtained using a reduced scaled charge, $q_{\mathrm{scaled}} = \pm 0.80e$. In this case, as mentioned in Sec. III A, all LJ parameters were

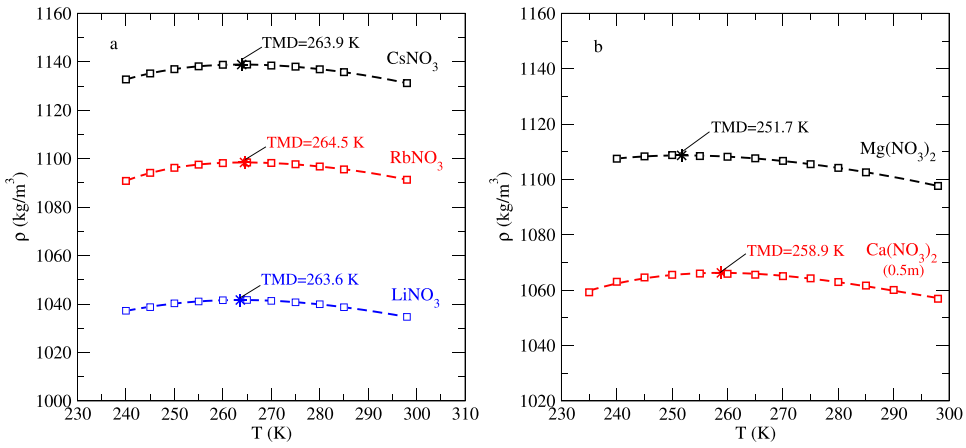

FIG. 4. Density as a function of temperature for aqueous nitrate salt solutions at a concentration of 1*m* and 1 bar (except for $Ca(NO_3)_2$ where the results were obtained for 0.5*m*). Panel (a): $CsNO_3$, $RbNO_3$, and $LiNO_3$; panel (b): $Mg(NO_3)_2$ and $Ca(NO_3)_2$. MD results are shown as open symbols and dashed lines, while dashed lines correspond to third-order polynomial fits to the MD data. The TMD obtained from the simulations is indicated by stars. All results were obtained using Model 5 with a net scaled charge for the nitrate anion and the cation of $q_{\mathrm{scaled}} = \pm 0.85e$.[15]

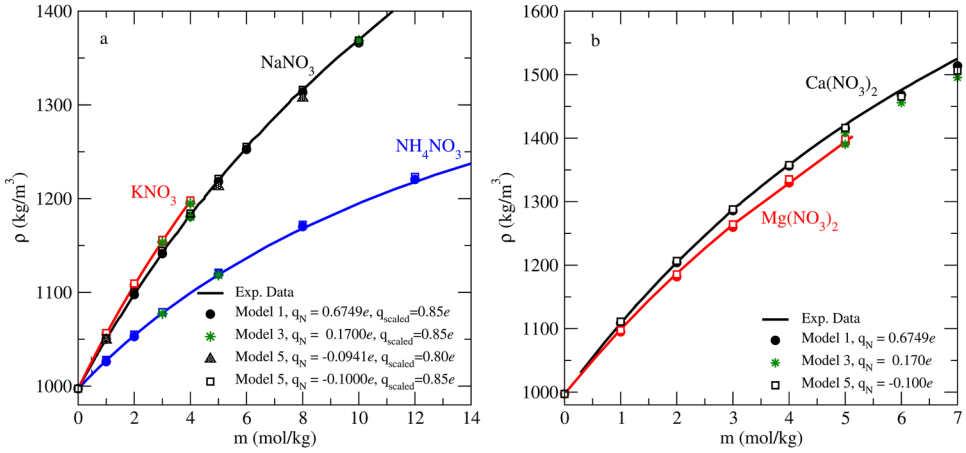

FIG. 5. Density as a function of molality for aqueous nitrate salt solutions at 298.15 K and 1 bar. Panel (a): $NaNO_3$, KNO_3, and NH_4NO_3; panel (b): $Ca(NO_3)_2$ and $Mg(NO_3)_2$. The simulation results are shown with symbols, while continuous lines stand for the experimental data taken from Refs. 67–69. The MD simulations were performed using the Models 1, 3, and 5 using a net scaled charge of $q_{scaled} = \pm 0.85e$ for both the nitrate anion and the cation.[15] For $NaNO_3$, additional simulations were carried out using $q_{scaled} = \pm 0.80e$ for both the nitrate anion and the Na^+ cation.

kept identical to those of the force field with $q_{scaled} = \pm 0.85e$, except for the value of σ for the Na^+–O_w interaction, which was previously optimized for $q_{scaled} = \pm 0.80e$.[12] As can be seen, the density predictions are only weakly affected by the intramolecular charge distribution over the entire range of molalities considered. In addition, Fig. 5(b) shows the density predictions for two divalent salts, $Mg(NO_3)_2$ and $Ca(NO_3)_2$, obtained using both models. For magnesium nitrate, Model 5 provides a remarkable agreement with experimental densities up to $5m$, demonstrating the robustness and transferability of the proposed nitrate nitrogen charge without the need to modify the LJ cross parameters (although this option is always possible if needed). The same is true for $Ca(NO_3)_2$. Overall, these results indicate that Model 5 provides a robust description of the density behavior of nitrate solutions without sacrificing the physical consistency of the original model. Once we have discussed the TMD and bulk densities, it seems of interest to compare Models 1 and 5 with respect to their transport properties. Model 5 would be of limited usefulness if it failed to accurately reproduce dynamical properties.

C. Transport properties

1. Self-diffusion coefficient

As shown in the previous figure, the TMD of aqueous nitrate salt solutions is sensitive to the intramolecular charge distribution of the nitrate ion. It is therefore of interest to assess how dynamical properties, such as self-diffusion and viscosity, are affected by this modification. To this end, the self-diffusion coefficients of water were computed for both Models 1 and 5 considered in this work. Accordingly, Fig. 6 presents a comparison between Models 1 and 5 for the self-diffusion coefficient of water, D_{H_2O}, as a function of molality for aqueous solutions of $NaNO_3$, KNO_3, and NH_4NO_3. For these three systems, experimental data for the water self-diffusion coefficient are scarce; the only available measurements correspond to KNO_3. As can be seen from Fig. 6(a), in the case of $NaNO_3$, both models predict a decrease in D_{H_2O} (dotted and dashed lines) with increasing salt concentration. Over the entire concentration range, the self-diffusion coefficients predicted by Models 1 and 5 are very similar. This behavior indicates that, for $NaNO_3$, the water self-diffusion coefficient is only weakly affected by variations in the nitrate nitrogen charge distribution. In the case of KNO_3, however, D_{H_2O} initially increases with molality, reaching a maximum around $1m$, and then decreases as the salt concentration continues to increase. To the best of our knowledge, experimental measurements of the water self-diffusion coefficient in KNO_3 solutions are limited to the studies by Tanaka[70] at 298.15 K in the low-concentration regime and by McCall *et al.*,[71] at 296.15 K up to $2.5m$. For KNO_3 [panel (b)], both models reproduce the experimental trend of the water self-diffusion coefficient at low concentrations, and a similar behavior of D_{H_2O} is observed for molalities in the range $1 \leq m \leq 3$. The experimental data at 296.15 K are included to illustrate that the simulation results follow the same overall concentration dependence observed experimentally. However, notice that these two experimental studies are not mutually consistent in the absolute values of the diffusion coefficient of water in the solution (two degrees cannot explain the difference in D for pure water in these two experimental studies). Nevertheless, the trend (i.e., the increase in the diffusion coefficient of water) is indeed found in both studies.

In contrast, for NH_4NO_3 [panel (c)], the self-diffusion coefficient of water is more strongly influenced by the nitrate nitrogen charge distribution. In this case, Models 1 and 5 exhibit similar overall trends, but noticeable differences in D_{H_2O} emerge at high molalities, indicating an enhanced sensitivity of water dynamics to the intramolecular charge distribution of the nitrate ion in the presence of the ammonium cation. In all cases, the values of D_{H_2O} obtained from the MD simulations at different salt concentrations were corrected for finite-size effects, as described in Sec. II D 1, by applying the hydrodynamic finite-size correction proposed by Yeh and Hummer.[52]

We have also calculated the diffusion coefficient of the nitrate anion at infinite dilution ($D^{\infty}_{NO_3^-}$), including YH corrections. This quantity was obtained by computing the self-diffusion coefficient of the nitrate anion at low molalities, that is, for concentrations below $1m$. For NO_3^-, the experimental self-diffusion coefficient at infinite dilution is $D^{\infty,exp}_{NO_3^-} = 1.90 \times 10^{-5}$ cm^2/s.[72] A comparison between the simulated values obtained with Models 1 and 5 and this experimental reference provides a good test of the force fields, as the experimental value is not influenced by the

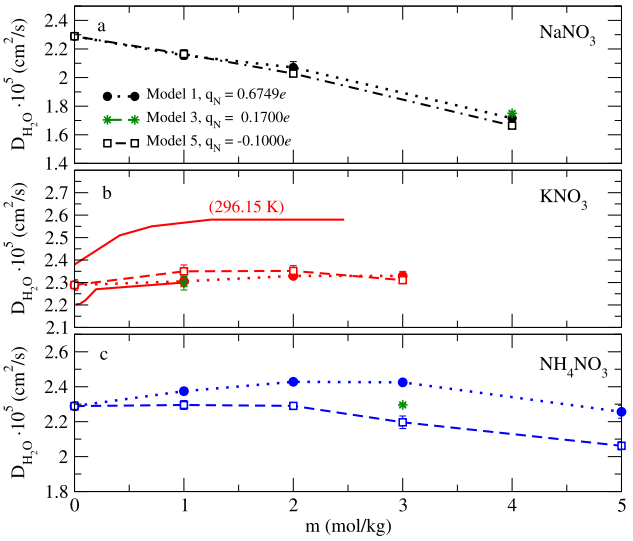

FIG. 6. Comparison between Models 1, 3, and 5 for the self-diffusion coefficient of water (D_{H_2O}) as a function of molality in aqueous nitrate salt solutions at 298.15 K and 1 bar. Panel (a): $NaNO_3$; panel (b): KNO_3; panel (c): NH_4NO_3. MD results are shown as filled symbols, while dashed and dotted lines are included as guides to the eye. The MD simulations were performed using a net scaled charge for the nitrate anion and the cation of $q_{scaled} = \pm 0.85e$.[15] Experimental data (continuous line) are shown in panel (b) for KNO_3, taken from Ref. 70 at 298.15 K and Ref. 71 at 296.15 K. All MD results include the hydrodynamic finite-size correction of Yeh and Hummer.[52]

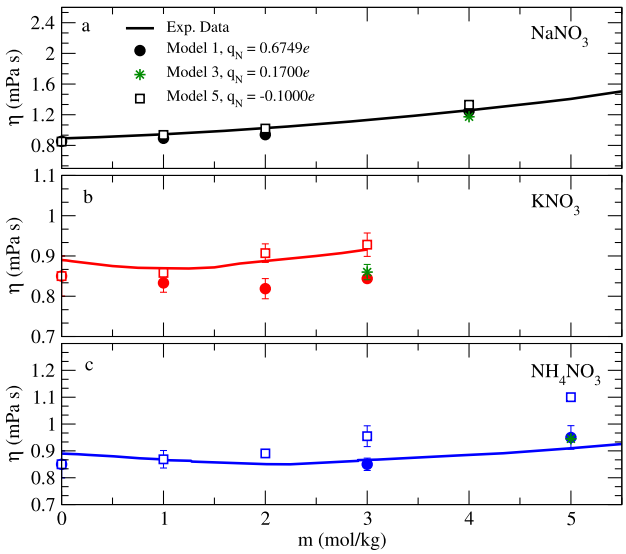

FIG. 7. Comparison between Models 1, 3, and 5 for the shear viscosity as a function of the molality in aqueous solutions of nitrate salts at 298.15 K and 1 bar. Panel (a): $NaNO_3$; panel (b): KNO_3; panel (c): NH_4NO_3 nitrate salts. MD results are shown as filled ($q_N = -0.6749e$[15]) and empty symbols ($q_N = -0.1000e$), while continuous lines represent experimental data taken from Ref. 23. The MD simulations were performed using a net scaled charge of $q_{scaled} = \pm 0.85e$ for both the nitrate anion and the cation.[15]

presence of counterions. The simulated values of $D^{\infty}_{NO_3^-}$, obtained by linear extrapolation of $D_{NO_3^-}$ for $NaNO_3$ in the limit $m \to 0$, show excellent agreement with experiment: $D^{\infty,sim}_{NO_3^-} = 1.987 \times 10^{-5}$ cm^2/s (deviation of 4.6%) for Model 1 and $D^{\infty,sim}_{NO_3^-} = 1.874 \times 10^{-5}$ cm^2/s (deviation of 1.4%) for Model 5.

2. Viscosities

After analyzing the TMD, densities, and the self-diffusion coefficient of water, the estimation of the shear viscosity constitutes the last dynamic property used to assess the performance of Model 5 in comparison with Model 1. For nitrate salt solutions, accurate experimental viscosity data are available over a wide range of molalities, allowing for a direct and meaningful comparison with MD simulations. Figure 7 shows a comparison between Models 1 and 5 for the shear viscosity as a function of molality at 298.15 K and 1 bar for $NaNO_3$, KNO_3, and NH_4NO_3. In the case of $NaNO_3$ (panel a), both models yield very similar viscosity values across the entire range of molalities studied. Consistently with the self-diffusion results, the dynamical properties of this salt in water are only weakly affected by the nitrate intramolecular charge distribution, indicating that the viscosity remains essentially unchanged between the two models. Figure 7(b) shows the shear viscosity for KNO_3. In this case, Model 5 significantly improves the prediction of the viscosity at both low and high concentrations, exhibiting excellent agreement with experimental data over the full molality range. The deviations from experimental values are below 2%, which is remarkable for a complex transport property such as shear viscosity. In panel (c), the results for NH_4NO_3 are shown. Here, Model 1 provides slightly better agreement with experimental data at molalities above $3m$, where the influence of the intramolecular charge distribution becomes more pronounced and larger deviations are observed for Model 5. Overall, these results indicate that Model 5 constitutes a reliable and transferable force-field parametrization for aqueous nitrate salt solutions. In most cases, the modified intramolecular charge distribution improves the prediction of both the TMD and shear viscosity, supporting its use in future studies. On the other hand, the ammonium ion (NH_4^+) is a multi-atomic species, and in principle, its properties could be influenced by its intramolecular charge distribution. However, unlike the nitrate ion, the ammonium ion has a non-planar, nearly tetrahedral geometry. This structural feature tends to reduce the sensitivity of its properties to variations in the charge distribution, as the charge is more symmetrically distributed. Recent work by Blazquez *et al.*[26] on a structurally similar non-planar ion, namely perchlorate, has shown that variations in the intramolecular charge distribution have only a minor impact on the predicted thermodynamic, structural, and dynamic properties. As a result, the system properties are expected to exhibit reduced sensitivity to the ammonium charge distribution. Furthermore, in ammonium nitrate (NH_4NO_3) solutions, the nitrogen atom of the ammonium ion does not interact with water as strongly or directionally as the nitrogen atom in the nitrate ion. As a result, the system properties are expected to be less sensitive to the ammonium charge distribution. Nevertheless, we acknowledge that a systematic analysis of the effect of charge distribution in ammonium could provide additional insights, but this aspect is beyond the scope of the present work and will be addressed in future studies.

The main conclusion of this section is that both models (Model 1 and Model 5) provide a reasonably accurate description of the

transport properties of aqueous nitrate solutions. The two models are essentially equivalent for $NaNO_3$; Model 5 performs slightly better for KNO_3, whereas Model 1 shows a slight advantage for NH_4NO_3. Since Model 5 yields superior predictions for the TMD, it appears to be the stronger candidate in the comparison between the two models. Nevertheless, before reaching a final decision, it is necessary to examine another key property in detail: the microscopic structure of the solutions.

D. Characterization of structural features

1. Radial distribution functions

The characterization of structural features in aqueous nitrate salt solutions is also of considerable interest, although experimental studies in this area remain scarce. A detailed analysis of structural properties, including radial distribution functions (RDFs), cation–anion organization, contact ion pairs, and hydration numbers for $NaNO_3$, KNO_3, and NH_4NO_3 has been previously reported in Ref. 15. For a system such as $NaNO_3$, there are 15 distinct atom–atom RDFs, making it impractical to display all of them. Therefore, we focus on correlations between the atoms of the nitrate group and the remaining species in the solution. In Fig. 8, we present the RDFs obtained with Models 1 and 5 for an aqueous $NaNO_3$ solution at a concentration of 4*m*, 298.15 K, and 1 bar. In Fig. 8(a), the top panel shows the N_n–Na^+ correlations, while the bottom panel displays the O_n–Na^+ correlations. The peak located around 5 Å corresponds to a solvent-shared ion pair (i.e., a Na^+ ion separated from the nitrate by a single water molecule). The shoulder at shorter distances provides evidence of some contact ion pairs, which appear in greater proportion for Model 5 than for Model 1. This behavior can be attributed to the negative charge assigned to the nitrogen atom in Model 5, which enhances electrostatic attraction. For the O_n–Na^+ interaction (bottom panel), a similar overall RDF is observed for both Models 1 and 5, indicating that the structural differences between the models are more pronounced in the N_n–Na correlations than in the O_n–Na ones.

Regarding the O_n–O_w RDF [Fig. 8(b), top panel], both models predict similar first-peak positions, namely 3.01 Å for Model 1 and 3.11 Å for Model 5. Neutron diffraction experiments[73,74] suggest that this distance should be close to 2.9 Å (it is important to note that the experiments do not allow a direct determination of the O_n–O_w distance; instead, it must be inferred from some type of geometrical model). For reference, this value is shown as a vertical line in the top panel of Fig. 8(b). In the bottom panel of Fig. 8(b), the O_n–H_w RDF exhibits first-peak positions at 2.05 Å for Model 1 and 2.22 Å for Model 5. Since the LJ parameters are identical in both models, the observed differences arise solely from the distinct charge distributions. In particular, the H_w atom approaches the O_n atom more closely in Model 1 than in Model 5 due to the larger (in absolute value) negative charge assigned to O_n in Model 1 ($q_{O_n} = -0.5083e$) as compared to Model 5 ($q_{O_n} = -0.2500e$).

Probably the most interesting discussion refers to correlations involving the nitrogen atom of the nitrate group, shown in Fig. 8(c). As expected, it is for these two correlation functions (N_n–O_w: top panel and N_n–H_w: bottom panel) where the results of the two models in this work differ more significantly (notice that Model 1 assigns a positive charge to the nitrogen atom, whereas Model 5 assigns a small negative charge). Consequently, the differences found in these RDFs reflect different ways of water solvating the nitrate anion. We show in the top panel of Fig. 8(c) with vertical lines the experimental positions of the first and second peaks of the N_n–O_w RDF, located at 2.65(5) and 3.40(10) Å, respectively, as reported by Neilson and Enderby.[74] In their paper, these authors propose a simple solvation model compatible with these peaks (see Fig. 3 of Ref. 74). According to this scheme, the peak at 2.65 Å is the distance between a molecule of water on the axial plane of the nitrate group (i.e., just on

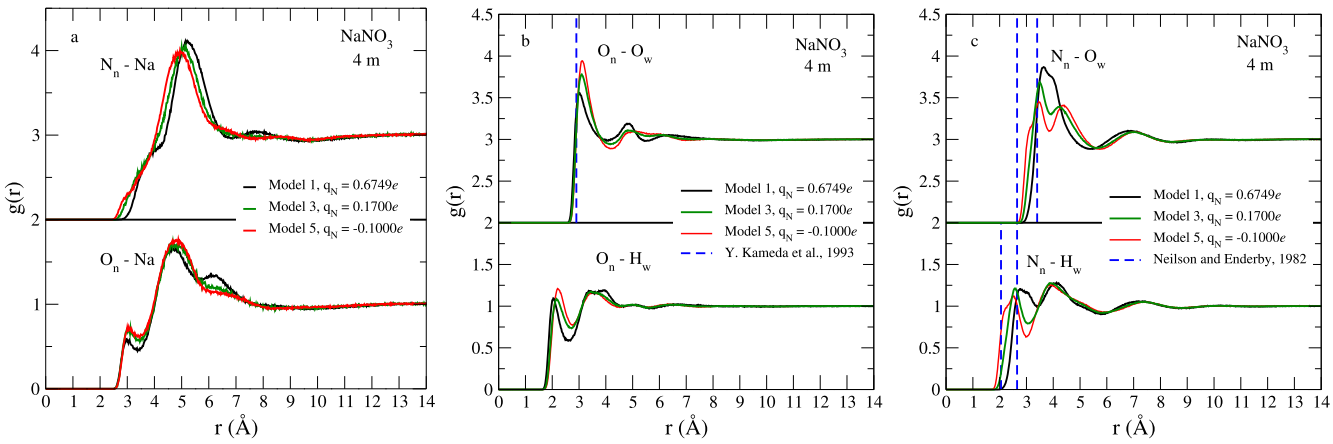

FIG. 8. Comparison between Models 1, 3, and 5 for the radial distribution functions (RDFs) for 4*m* $NaNO_3$ solutions at 298.15 K and at 1 bar. Panel (a): N_n–Na and O_n–Na correlations; panel (b): O_n–O_w and O_n–H_w correlations; and panel (c): N_n–O_w and N_n–H_w correlations. The MD simulations were performed using a net scaled charge of $q_{scaled} = \pm 0.85e$ for both the nitrate anion and the Na^+ cation.[15] Continuous lines represent the RDFs obtained from the simulations, while dashed lines indicate the positions of the first and second peaks in the experimental RDFs. Experimental data are taken from Refs. 73 and 74 for the O_n–O_w interaction and from Ref. 74 for the N_n–O_w and N_n–H_w interactions. In panels (a)–(c), RDFs obtained with Model 3 are also included to illustrate its intermediate behavior. In the upper panels, the RDFs have been vertically shifted by two units for clarity.

the top of the nitrogen atom), while the distance 3.40 Å corresponds to the distance between the nitrogen and a molecule of water on the equatorial position (the reported uncertainty for the precise location of these peaks is ~0.1 Å). Note that Model 5 is compatible with these experimental findings (i.e., the first peak exhibits a shoulder at short distances compatible with the existence of two peaks). The first peak of Model 5 reflects the molecules of water directly solvating the nitrate anion, whereas the second peak (at 4.40 Å) corresponds to the second solvation shell. In contrast, Model 1 displays a broad peak involving molecules of the first and second solvation shells and is unable to describe the experimental peak found at 2.65 Å. Previous simulation studies report a wide range of values for the position of the first maximum of the N_n–O_w RDF: 3.4–3.5 Å from polarizable force fields,[75,76] and 3.68 Å from reference interaction site model self-consistent field (RISM-SCF) calculations.[77] Classical nonpolarizable simulations yield N_n–O_w distances of ~3.50 Å for rigid models[78] and 3.48 Å for flexible models.[8] However, almost all these studies use force fields with a large positive charge on the location of the nitrogen group, thus resembling our results here for Model 1. The negative charge assigned to the nitrogen atom in Model 5 ($q_N = -0.1000e$) enhances nitrate–water interactions, allowing water coordination in both radial and axial directions, and leads to shorter N_n–O_w distances as a result of reduced electrostatic repulsion. Finally, in Fig. 8(c) (bottom panel), we present the RDF for the N_n–H_w interaction. For comparison, we include the experimental positions of the first and second peaks of the N_n–H_w RDF, located at 2.05(2) and 2.65(10) Å, respectively, as reported in Ref. 74. According to Neilson and Enderby,[74] these two distances correspond to the distance of the nitrogen atom to the hydrogen on the axial position (2.05 Å) and to the hydrogens of the water molecules on the equatorial positions (2.65 Å). Our results for Model 5 are compatible with these two distances, as the first peak contains a clear shoulder and can be described as the result of two contributions. The second peak in Model 5 corresponds to hydrogens not pointing toward the nitrate group within the first solvation shell, as well as contributions from the hydrogens of the second solvation shell.

We now proceed to compute the hydration number of the nitrate anion. For this purpose, an expanded version of the N_n-O_w and N_n–H_w RDFs is presented in Fig. 9. The number of water molecules around the nitrate group can be obtained by integrating the N_n–O_w RDF [see Fig. 9(a)] up to its first minimum. For Model 5, there is a well-defined minimum in this RDF at 3.9 Å, so that we shall integrate until the first minimum, resulting in a coordination number of 5. Therefore, Model 5 predicts a hydration number of five water molecules, in excellent agreement with the structural picture described by Neilson and Enderby,[74] namely, three water molecules solvating in the equatorial plane and two of them solvating in the axial plane of the nitrate group. Typically, when computing the hydration number one integrates the RDF until the first minimum (as we have done with Model 5). However we do the same for Model 1, where the first minimum is located at 5.5 Å, one would obtain an unrealistically large hydration number, which is obviously wrong. The problem is that in Model 1, the first and second solvation shells overlap. It makes more sense to integrate for Model 1 only up to the distances where the minimum appears in Model 5 in order to compute the hydration number. Using this criterion, Model 1 also yields a hydration number of 5. Notice also the existence of a small shoulder in the first peak of Model 1 located around 3.9 Å, probably indicating the crossing from the first to the second solvation shells. Thus, our results strongly suggest 5 as the hydration number of the nitrate group (i.e., the number of water molecules in contact with the anion).

Let us now try to estimate the hydration number from the number of hydrogen atoms around the N_n atom. For Model 5, we obtained 4.15 by integrating up to the first minimum. The physical picture is that the three water molecules solvating the O_n in the equatorial position have one hydrogen atom pointing toward the O_n atom. On the other hand, for the two axial molecules of water, half of the time they have one hydrogen pointing toward the N_n and half of the time they have both two H atoms pointing toward the solution. In this way, one can explain 5 molecules of water and 4 H atoms for the solvation around the N_n. However, in the case of Model 1, the first minimum appears at larger distances and the integral yields a number of seven. In this case, again 3 hydrogens of water points toward the O_n in the equatorial plane, and the two molecules of water of the axial plane have their hydrogens toward the solution and not toward the N_n atom, so that one obtains a total of 7 hydrogen atoms. It is clear that Models 1 and 5 differ significantly

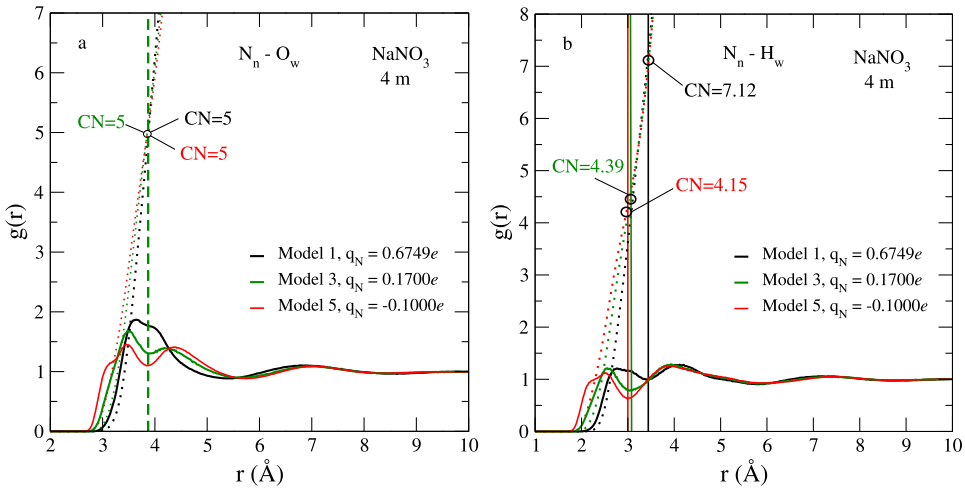

FIG. 9. Coordination numbers of Models 1, 3, and 5 for the RDFs for 4*m* $NaNO_3$ solutions at 298.15 K and 1 bar. Panel (a): N_n–O_w; and panel (b): N_n–H_w correlations. The MD simulations were performed using a net scaled charge of $q_{scaled} = \pm 0.85e$ for both the nitrate anion and the Na^+ cation.[15] Continuous lines represent the RDFs obtained from the simulations, while vertical lines indicate the position of the first minimum in the RDF.

in the way the water molecules are solvating the nitrate group, especially in the orientation of the water molecules located on the perpendicular to the plane of the anion.

Overall, the results of Model 5 provide a more consistent description of the experimental results reported by Neilson and Enderby.[74] However, the paper of Neilson and Enderby is relatively old (1982), and in addition, their interpretation involves assigned peaks in the neutron diffraction to a certain RDF, which involves some degree of uncertainty. Furthermore, obtaining all RDFs from diffraction techniques is practically impossible. Fortunately, in 2018, there was a new experimental study on neutron diffraction of a nitrate salt[79] that allowed for the determination of the global $G(r)$ for O_n and N_n [the meaning of $G(r)$ will be explained in Sec. III D 2], so that one can compare without ambiguity the global $G(r)$ from simulations with the global $G(r)$ from experiments. This comparison is presented in Subsection III D 2.

2. Comparison with neutron diffraction

Over the past decades, experimental techniques such as X-ray and neutron diffraction have been increasingly employed to obtain detailed structural information on aqueous solutions, particularly regarding how atoms interact at the microscopic level, as characterized by RDFs. Among these techniques, neutron diffraction, especially when combined with isotope substitution, provides direct access to partial pair correlation functions and offers valuable insight into the hydration structure of dissolved ions. Consequently, neutron diffraction data constitute an important benchmark for validating MD simulations of aqueous electrolyte solutions. In particular, neutron diffraction with isotopic substitution (NDIS) is especially powerful for disentangling specific atomic correlations.[80–83] By performing diffraction experiments with two nitrogen isotopes in the nitrate group dissolved in deuterated water, the difference of the structure factors is due uniquely to five atom–atom correlation functions, two of which have a large weight, namely, the N–O_w (where the subscript w refers to the oxygen of water) and the N–D (D being the deuterium atom). That was done for nitrate anions by Neilson and Enderby for the first time,[74] and followed by others.[73,79] A similar approach can be used by replacing two isotopes of the oxygen atom in the nitrate group.[79] The problem with the NDIS technique is that what one obtains is the total RDF, $G(r)$, which is a combination of several atom–atom RDFs, so that one must "interpret/assign" each peak to a certain atom–atom RDF or to a combination of them.

Recently, NDIS experimental diffraction results have been published for aqueous KNO_3 at a concentration of 3.4m, T = 298.15 K, and 1 bar,[79] using both isotope replacement for the N in one set of experiments and for the O_n in another set. In the case of isotope substitution of O_n, the experimental diffraction data allow the determination of $G_{O_n}(r)$ defined as (weights are provided for the particular case of the KNO_3 3.4m solution)

$$G_{O_n}(r) = 0.63g_{O_n-H_w}(r) + 0.28g_{O_n-O_w}(r) + 0.05g_{O_n-O_n}(r) + 0.03g_{O_n-N_n}(r) + 0.01g_{O_n-K}(r), \quad (3.5)$$

where $g_{O_n-\alpha}(r)$ is the RDF distribution function between the oxygen atom of the nitrate group O_n and an atom of type α in the system. In the case of isotope substitution of N, the experimental diffraction data allow the determination of the function $G_N(r)$ defined as (weights are provided for the particular case of the KNO_3 3.4m solution)

$$G_N(r) = 0.64g_{N_n-H_w}(r) + 0.28g_{N_n-O_w}(r) + 0.05g_{N_n-O_n}(r) + 0.02g_{N_n-N_n}(r) + 0.01g_{N_n-K}(r), \quad (3.6)$$

where $g_{N_n-\alpha}$ is the RDF between the nitrogen atom of the nitrate group and an atom of type α of the system.

To determine the functions $G_{O_n}(r)$ and $G_N(r)$ from simulations, we performed MD simulations of aqueous KNO_3 at 3.4m, T = 298.15 K, and 1 bar for Models 1 and 5, and computed all atom-atom RDF distribution functions in the system, and calculated the corresponding $G(r)$. We can now compare the simulation with the experimental results. It should be mentioned, though, that the experiments are performed with D_2O, and the structure of D_2O is not identical to that of H_2O, which could slightly impact some of the results. Panels (a) and (b) of Fig. 10 show the five individual contributions to $G_{O_n}(r)$ arising from correlations between the nitrate oxygen atoms (O_n) and H_w, O_w, O_n, K^+, and N_n for Models 1 and 5, respectively, and the sum of all of them (red line), which can be compared with the experimental results (black solid line and open circles). The results of both models are similar, although it seems that the results of Model 1 are somewhat superior. At short distances (below 2.5 Å), the only non-zero RDF is the O_n–H_w RDF contribution. It seems that in experiments, the hydrogen atoms get closer to the O_n group than in the results of the simulations using the two force fields of this work. As the hydrogen atom of water has no LJ center, to improve the agreement with experiment, a slightly lower value of σ for the O_n–O_w interaction would be beneficial. Panels (c) and (d) display the corresponding contributions involving the nitrate nitrogen atom (N_n) and the same species. In this particular case, the agreement found for Model 1 seems to be better than that found for Model 5. In Model 5, the hydrogen atoms get closer to the N_n, probably due to the positive charge of hydrogen in the water force field and to the negative charge of N_n in Model 5. Having a positive charge on the nitrogen and probably increasing slightly the σ for the N_n–O_w could improve agreement with experiment. In any case, the results shown in Fig. 10 indicate that, overall, Model 1 provides a more accurate structural description than Model 5.

IV. SUGGESTED FORCE FIELD

The TMD has recently emerged as a key thermodynamic benchmark for assessing force-field performance for pure water and aqueous salt solutions. Improving its prediction has therefore become an important target in force-field development, subject to the availability of reliable experimental data. As reported by the authors in Ref. 23, the extended parametrization of the Madrid model for nitrate salts ($NaNO_3$, KNO_3, and NH_4NO_3, referred to as Model 1) exhibits deviations of 6.3 K at 1m in the prediction of the TMD. Deviations of this magnitude had not previously been observed in TMD predictions for electrolyte solutions using the Madrid-2019 force field.[12,24,25] This issue motivated the present study, in which we explored whether modifying the intramolecular charge distribution of the nitrate ion could improve the prediction of the TMD while preserving the overall quality and physical consistency of the force field.

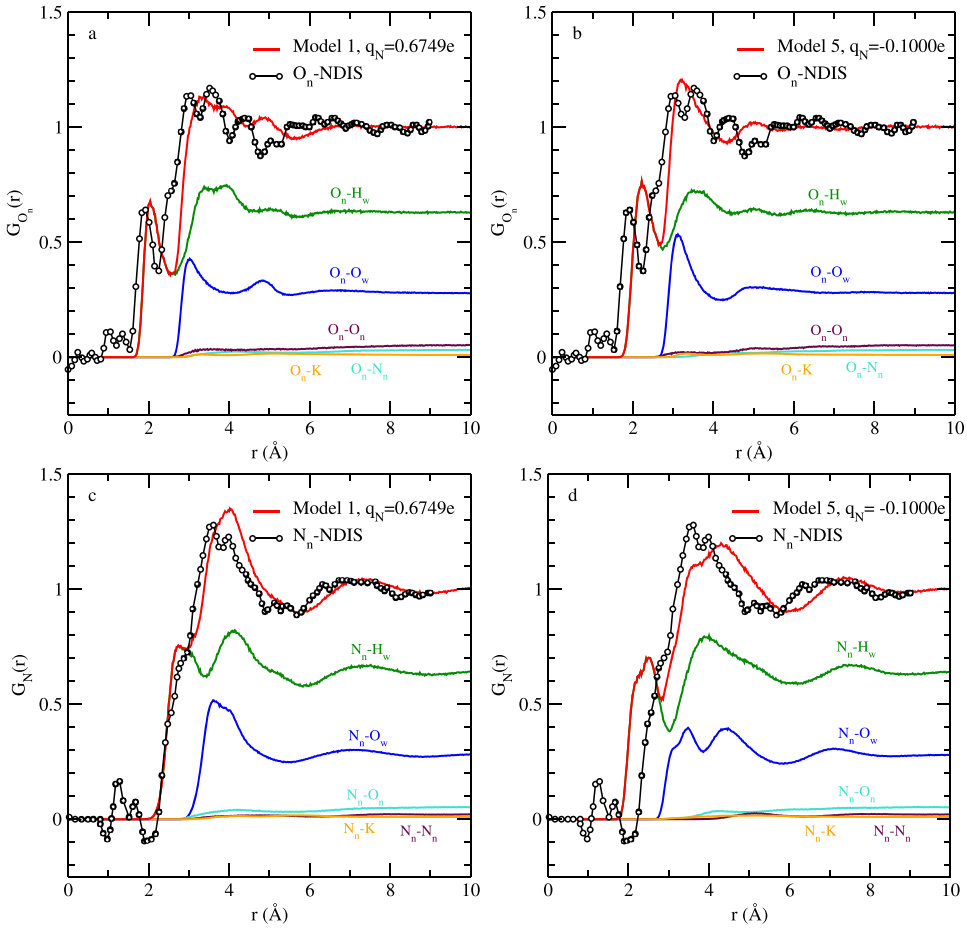

FIG. 10. Panels (a) and (b): Contributions to $G(r)$ arising from correlations between the nitrate oxygen atoms (O_n) and H_w, O_w, O_n, K^+, and N_n for Models 1 and 5, respectively. Panels (c) and (d): the same as in panels (a) and (b) but for the corresponding contributions involving the nitrate nitrogen atom (N_n) and the same species. Experimental data are taken from Ref. 79.

Then, we reparametrized the nitrate ion (NO_3^-) by proposing five intramolecular charge distributions, while maintaining a net scaled charge of $q_{\text{scaled}} = \pm 0.85e$ and keeping the cation parameters unchanged from the Madrid-2019 force field.[11,15,35] Based on the TMD predictions, we identified Model 5 ($q_N = -0.1000e$) as the one providing the best agreement with experiment for the TMD. In this model, the nitrogen atom carries a partial charge of $q_N = -0.1000e$, while the oxygen atoms carry charges of $q_{O_n} = -0.2500e$. This is in contrast with our original model for the nitrate anion, Model 1, ($q_N = 0.6749e$),[15] that differs only in the intramolecular charge distribution of the nitrate ion. The LJ parameters are the same for all models, highlighting that the observed differences arise exclusively from changes in the charge distribution. Using Model 5, we provide predictions of the TMD for several nitrate salts for which experimental values have not yet been reported. Furthermore, we estimate the Despretz constant for the nitrate group as -11.4 K kg mol^{-1}. To further test whether the improvement in the TMD deteriorates other properties, we tested the densities of concentrated nitrate solutions and found that Model 5 provides results as good for densities as our original Model 1. Thus, the global density is not very sensitive to the intramolecular charge distribution. We then tested transport properties and found that transport properties of Model 1 and Model 5 were also similar (although not identical). It seems that, in general, the viscosities of Model 1 were slightly lower than those of Model 5 (with almost identical results for $NaNO_3$, somewhat better agreement with experiment for Model 5 in the case of KNO_3, and slightly better agreement with experiment for Model 1 in the case of NH_4NO_3). We were even able to describe an increase in the diffusion coefficient of water with the addition of KNO_3, in agreement with the experimental results reported some time ago.

An intermediate model (such as Model 3 in this work) can therefore be considered a reasonable choice for the nitrate force field, as it improves the prediction of the TMD relative to Model 1 while preserving structural features more accurately than Model 5. Figure 11 shows the total contributions to $G_{O_n}(r)$ and $G_N(r)$, obtained from the sum of individual pair correlations involving nitrate oxygen atoms (O_n) with H_w, O_w, O_n, K^+, and N_n, for Models 1, 3, and 5. The results correspond to a KNO_3 aqueous solution at a concentration of 3.4m. As observed in panel (a), all three models yield similar trends; however, Models 1 and 3 exhibit slightly better agreement with the experimental data than Model 5, particularly in the first coordination shell. In panel (b), Model 1 shows the best overall agreement with the experimental curve, although Model 3 provides a more accurate description in the region

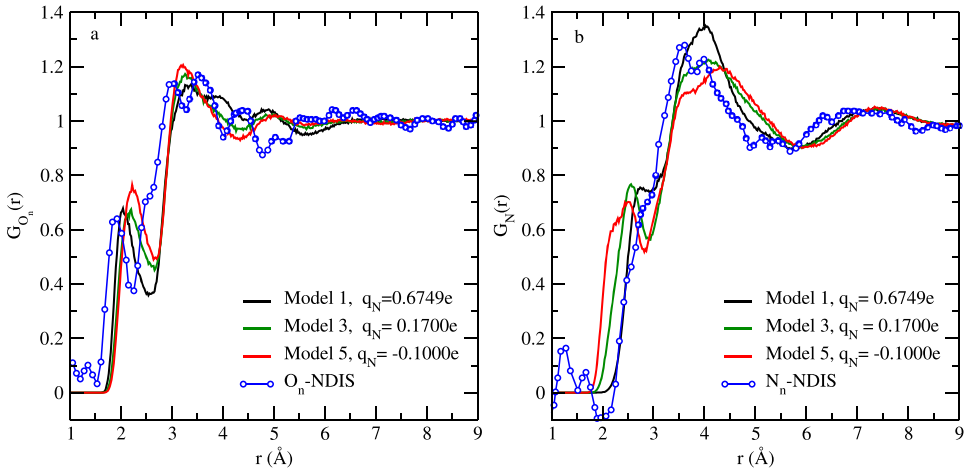

FIG. 11. Panel (a): Contributions to $G(r)$ arising from correlations between the nitrate oxygen atoms (O_n) and H_w, O_w, O_n, K^+, and N_n for Models 1, 3, and 5, respectively. Panel (b): the same as in panel (a) but for the corresponding contributions involving the nitrate nitrogen atom (N_n) and the same species. The results correspond to a KNO_3 aqueous solution at a concentration of 3.4*m*. Experimental data are taken from Ref. 79.

of the main peak. Model 5, in contrast, displays larger deviations in both panels. Overall, Model 3 represents a balanced compromise: while it does not consistently outperform Model 1 in structural predictions, it significantly improves upon Model 5 and offers a better combined description of thermodynamic and structural properties.

This conclusion is consistently supported throughout the manuscript. First, in Table V, we present a comparison of the TMD and the corresponding density at the TMD for the three studied salts using Models 1, 3, and 5. Second, in Fig. 5, density calculations for all studied monovalent and divalent salts are reported, showing that Models 1, 3, and 5 provide almost identical and accurate density predictions. Third, in Fig. 6, we include calculations of the self-diffusion coefficient of water for the NH_4NO_3 system using Model 3, while Fig. 7 presents shear viscosity results for the three salts using the same model. In all cases, Model 3 exhibits intermediate behavior relative to Models 1 and 5. Thus, both transport properties and densities predicted by Model 3 fall between those obtained with Models 1 and 5, indicating that it provides a reasonable compromise between accuracy and transferability. In Fig. 8, we include RDF predictions obtained with Model 3, demonstrating that the structural properties are also reasonably well reproduced by this model. Finally, we have computed (for Models 1, 3, and 5) the water–water and ion–water energies in a 1*m* solution of KNO_3 at 298.15 K and 1 bar, as it has been shown recently that these energies are useful to understand the structural changes that ions provoke in the structure of water (see details in Ref. 84). Results are presented in Table VI. Both water–water and ion–water energies are similar for the three models. Model 1 disrupts the water–water energy more (as compared to pure water) and exhibits a slightly less favorable ion–water energy when compared to Model 5, with the behavior of Model 3 being intermediate.

The partial charges of Model 3 are similar to those that would have been obtained from quantum chemistry when using the Hirshfeld method. Model 3 uses the same LJ parameters as Model 1, as densities and the rest of the properties are well predicted even after changing the partial charges. In the supplementary material, we have included the TMD by using Model 3 with slightly modified LJ parameters showing that the conclusions of this work would not be modified by an additional optimization of the LJ parameters for Model 3.

TABLE VI. Water–water and ion–water interaction energies at 298.15 K and 1 bar for a 1*m* KNO_3 aqueous solution, obtained using Models 1, 3, and 5. Energies (in kJ/mol) are normalized per mol of water molecules (except in the last column where the ion–water energy is also presented per mol of salt). In pure water, the water–water interaction energy under these conditions is −47.85 kJ/mol. Note that the ion-water energies include contributions from both nitrate and potassium ions.

Model	Water-water	Ion-water	Ion-water
1	−41.77(2)	−11.76(4)	−652(2)
3	−41.79(2)	−11.77(4)	−653(2)
5	−41.83(2)	−11.91(4)	−661(2)

V. CONCLUSIONS

One of the main conclusions of this work is that the overall density is not highly sensitive to the intramolecular charge distribution, while transport properties are only moderately affected. In contrast, the TMD is significantly influenced by the charge distribution, particularly considering that the nitrate ion is a planar molecule where all the atoms of the ion are in contact with water. With all this information together, one concludes that Model 5 is as good as Model 1 for all properties, but it has the advantage of improving the predictions of the Temperature of Maximum Density (TMD). However, after analyzing structural properties, it was found that Model 5 modified the way water solvates the nitrate group. Although in both Models 1 and 5 the partial charges of the oxygen atoms of the nitrate ion are negative, the charge on the nitrogen atom is positive in Model 1 and negative in Model 5. This difference modifies dramatically the way water is solvating the nitrate anion. Although Model 5 seems to be consistent with the structural model proposed many years ago by Neilson and Enderby[74] from the analysis of neutron diffraction data, it is clear that when one analyzes the more recent experimental[79] results (obtained from NDIS), the structural predictions of Model 1 seem superior. Thus, this strongly suggests that the predictions of Model 1 for structure are superior to

those of Model 5. This result indicates that improvements in thermodynamic properties do not necessarily translate into uniformly better agreement with all structural observables (in agreement with a recent study of $CaCl_2$ aqueous solutions where similar conclusions were reached[85]). We should also mention that NDIS describes the structure of water around the ions, but this is only half of the story, as it is also necessary to take into account the structural changes of water provoked by the presence of the ions to have a complete perspective of the structural changes. For instance, the ion–oxygen of water distances of the Madrid-2019 are in general slightly smaller than the experimental values for alkaline metals and for halogens. However, this small "shift" is compensated by an overall better performance, thus reflecting that it is not only important to describe the behavior of the water in contact with the ion but also that of water beyond the first hydration layer.

Although additional properties, such as freezing-point depression, dielectric constants, and, recently, aqueous solubility,[86] should be investigated as important targets to fully assess the overall performance of the force field, the results presented here support the use of Model 5 for nitrate ions when the accurate prediction of the TMD is a primary objective. Conversely, Model 1 may be preferred when the primary objective is an accurate description of the structural properties of the system. Unfortunately, neither of these two models is capable of describing both properties simultaneously. A similar situation was found in a recent paper dealing with force fields for $CaCl_2$ in water, which showed that the model better describing the thermodynamic properties was not the best when describing structural properties.[85] This limitation reflects the inherent constraints of non-polarizable force fields. That said, both Model 1 and Model 5 perform reasonably well in describing the densities of concentrated solutions and their transport properties. At first sight, the results of this work are somewhat deceptive, as no model is able to reproduce all the experimental properties of nitrate solutions. It is worth noting that even for pure water, it has proven impossible to develop non-polarizable models that simultaneously reproduce both the TMD and the melting temperature, which highlights the limitations of this class of models when describing aqueous electrolytes. That being true, it must also be stressed that both Models 1 and 5 are able to describe reasonably well the densities, the infinite dilution diffusion coefficient, the viscosities, and the TMD of many nitrate salts, and they can be taken as reasonable force fields for nitrate. Then, we recommend Model 3 as a reasonable choice for the nitrate group force field, as it improves the predictions of the TMD with respect to Model 1 while preserving its structural predictions; that is, Model 3 represents a compromise. Note that, although Model 3 (and the Madrid-2019 force field in general) was originally optimized for the TIP4P/2005 water model, it has recently been shown that it can also be used with the TIP4P/ICE water model,[87] provided that the same LJ parameters are applied for the ion–water cross interactions.[88]

Recently, machine-learning-based potentials have experienced remarkable growth in the study of ionic solutions and water-like systems, combining electronic structure calculations with the computational efficiency of empirical force fields.[89] These advances have enabled significant progress in modeling water and aqueous systems across different length and time scales. It remains to be seen the success of these methods to reproduce all the properties addressed in this work: TMD (both temperature and density at the maximum), densities of solutions up to high concentrations, viscosities, diffusion coefficients, and the description of the structure as obtained from NDIS techniques. Time will tell how these new approaches perform in reproducing all these properties simultaneously. For the time being, Model 3 provides a reasonably good description of the behavior of ionic aqueous solutions containing the nitrate anion.

DEDICATION

We are deeply honored to dedicate this work to Professor Christoph Dellago. We gratefully acknowledge his intellectual leadership in the study of crystal structures, phase transitions, stochastic thermodynamics, and nucleation processes, as well as his friendship over the years.

SUPPLEMENTARY MATERIAL

In the supplementary material, we provide the raw simulated data and graphical results obtained from the MD simulations of the nitrate salts investigated in this work for different values of the nitrate nitrogen charge (q_N). The following properties are shown: (i) Contributions to $G(r)$ arising from correlations between nitrate oxygen atoms (O_n) and nitrate nitrogen atoms (N_n) with H_w, O_w, O_n, K^+, and N_n for Models 3 and 4. (ii) Raw simulated densities as a function of temperature for aqueous $NaNO_3$ solutions at a concentration of $1m$ and room pressure, for different values of the nitrate nitrogen charge (q_N). (iii) Raw simulated temperature of maximum density (TMD) and the corresponding density at the TMD as a function of q_N for aqueous $NaNO_3$ solutions. (iv) Raw simulated densities as a function of temperature for aqueous salt solutions of KNO_3 and NH_4NO_3. (v) Raw simulated densities as a function of molality for aqueous nitrate salt solutions ($NaNO_3$, KNO_3, NH_4NO_3, $Ca(NO_3)_2$, and $Mg(NO_3)_2$). (vi) Raw simulated self-diffusion coefficient of water (D_{H_2O}) and shear viscosity (η) as a function of molality in aqueous nitrate salt solutions ($NaNO_3$, KNO_3, and NH_4NO_3). (vii) Raw simulated shear viscosity (η) as a function of molality in aqueous nitrate salt solutions ($NaNO_3$, KNO_3, and NH_4NO_3) using the Model 5. (viii) Raw simulated densities as a function of temperature for aqueous salt solutions of $CsNO_3$, $RbNO_3$, $LiNO_3$, $Ca(NO_3)_2$, and $Mg(NO_3)_2$. (ix) Summary of the crossed LJ (σ_{ij}, ε_{ij}) parameters for the original force field and for a modified trial version (LJ modified). (x) Contributions to $G(r)$ arising from correlations between nitrate oxygen atoms (O_n) and nitrate nitrogen atoms (N_n) with H_w, O_w, O_n, K^+, and N_n for Models 1, 3, 3 (LJ modified), and 4. (xi) Density as a function of molality for aqueous nitrate salt solutions ($NaNO_3$, KNO_3, and NH_4NO_3) at 298.15 K and 1 bar. (xii) Raw calculated values of the TMD and the corresponding density at the TMD (ρ_{max}) for aqueous salt solutions at $1m$ concentration and room pressure, for $NaNO_3$, KNO_3, and NH_4NO_3. In addition, the MD input files, *topol.top* and *conf.g96*, are included for reference and to ensure reproducibility of the simulations.

ACKNOWLEDGMENTS

V.M.T. and M.C.-S. acknowledge financial support from SECIHTI-Mexico through the program "Convocatoria Ciencia Básica y de Frontera 2023-2024" Grant No. CBF2023-2024-2725, Proyecto PEAPDI2025 "Modelado molecular de disoluciones

electrolíticas con disolvente agua–metanol. Dependencia sobre la temperatura, presión y composición," Proyecto PEAPDI2025 "Síntesis y Caracterización de Estructuras Mesoporosas de Carbono," and the Department of Physical Chemistry at the Universidad Complutense de Madrid for its hospitality. The authors also thank funding through the Ministerio de Ciencia e Innovación de España (Grant Nos. PID2022-136919NB-C31, PID2022-136919NA-C33, and PID2025-168591NB-I00).

AUTHOR DECLARATIONS

Conflict of Interest

The authors have no conflicts to disclose.

Author Contributions

M. Cruz-Sánchez: Conceptualization (equal); Data curation (equal); Investigation (equal); Writing – original draft (equal); Writing – review & editing (equal). **F. Gámez**: Conceptualization (equal); Data curation (equal); Writing – original draft (equal); Writing – review & editing (equal). **C. Vega**: Conceptualization (equal); Formal analysis (equal); Investigation (equal); Supervision (equal); Writing – original draft (equal); Writing – review & editing (equal). **V. M. Trejos**: Conceptualization (equal); Formal analysis (equal); Investigation (equal); Supervision (equal); Writing – original draft (equal); Writing – review & editing (equal).

DATA AVAILABILITY

The data that support the findings of this study are available within the article and its supplementary material.

REFERENCES

[1] B. Elvers, S. Hawkins, and W. Russey, *Ullmann's Encyclopedia of Industrial Chemistry* (Wiley Online Library, 1989).
[2] W. Laue, M. Thiemann, E. Scheibler, and K. W. Wiegand, "Nitrates and nitrites," Ullmann's Encycl. Ind. Chem. **24**, 153–157 (2000).
[3] J. Hagin, S. R. Olsen, and A. Shaviv, "Review of interaction of ammonium - nitrate and potassium nutrition of crops," J. Plant Nutr. **13**(10), 1211–1226 (1990).
[4] J. Fanning, "The chemical reduction of nitrate in aqueous solution," Coord. Chem. Rev. **199**(1), 159–179 (2000).
[5] P. Brimblecombe and D. H. Stedman, "Historical evidence for a dramatic increase in the nitrate component of acid rain," Nature **298**(5873), 460–462 (1982).
[6] M. E. E. Alahi and S. C. Mukhopadhyay, "Detection methods of nitrate in water: A review," Sens. Actuators, A **280**, 210–221 (2018).
[7] W. F. van Gunsteren, D. Bakowies, R. Baron, I. Chandrasekhar, M. Christen, X. Daura, P. Gee, D. P. Geerke, A. Glättli, P. H. Hünenberger, M. A. Kastenholz, C. Oostenbrink, M. Schenk, D. Trzesniak, N. F. A. van der Vegt, and H. B. Yu, "Biomolecular modeling: Goals, problems, perspectives," Angew. Chem., Int. Ed. **45**, 4064–4092 (2006).
[8] S. Mosallanejad, I. Oluwoye, M. Altarawneh, J. Gore, and B. Z. Dlugogorski, "Interfacial and bulk properties of concentrated solutions of ammonium nitrate," Phys. Chem. Chem. Phys. **22**, 27698–27712 (2020).
[9] D. Schaefer, M. Kohns, and H. Hasse, "Molecular modeling and simulation of aqueous solutions of alkali nitrates," J. Chem. Phys. **158**(13), 134508 (2023).
[10] C. P. Lamas, C. Vega, and E. G. Noya, "Freezing point depression of salt aqueous solutions using the Madrid-2019 model," J. Chem. Phys. **156**(13), 134503 (2022).
[11] I. M. Zeron, J. L. F. Abascal, and C. Vega, "A force field of Li^+, Na^+, K^+, Mg^{2+}, Ca^{2+}, Cl^-, and SO_4^{2-} in aqueous solution based on the TIP4P/2005 water model and scaled charges for the ions," J. Chem. Phys. **151**, (13), 134504 (2019).
[12] S. Blazquez, M. M. Conde, and C. Vega, "Scaled charges for ions: An improvement but not the final word for modeling electrolytes in water," J. Chem. Phys. **158**(5), 054505 (2023).
[13] S. Blazquez, J. L. F. Abascal, J. Lagerweij, P. Habibi, P. Dey, T. J. H. Vlugt, O. A. Moultos, and C. Vega, "Computation of electrical conductivities of aqueous electrolyte solutions: Two surfaces, one property," J. Chem. Theory Comput. **19**, 5380–5393 (2023).
[14] M. A. Gonzalez, D. Carrasco-Busturia, C. Vega, and J. L. F. Abascal, "Large scale simulations of a detailed molecular model of seawater: Ionic conductivity and diffusion coefficients of CO_2," J. Chem. Phys. **163**(3), 034505 (2025).
[15] V. M. Trejos, M. de Lucas, C. Vega, S. Blazquez, and F. Gámez, "Further extension of the Madrid-2019 force field: Parametrization of nitrate (NO_3^-) and ammonium (NH_4^+) ions," J. Chem. Phys. **159**(22), 224501 (2023).
[16] Y. Yao, M. L. Berkowitz, and Y. Kanai, "Communication: Modeling of concentration dependent water diffusivity in ionic solutions: Role of intermolecular charge transfer," J. Chem. Phys. **143**(24), 241101 (2015).
[17] Y. Yao and Y. Kanai, "Free energy profile of NaCl in water: First-principles molecular dynamics with SCAN and ωB97X-V exchange–correlation functionals," J. Chem. Theory Comput. **14**, 884–893 (2018).
[18] B. J. Kirby and P. Jungwirth, "Charge scaling manifesto: A way of reconciling the inherently macroscopic and microscopic natures of molecular simulations," J. Phys. Chem. Lett. **10**, 7531–7536 (2019).
[19] M. Jorge, "Theoretically grounded approaches to account for polarization effects in fixed-charge force fields," J. Chem. Phys. **161**(18), 180901 (2024).
[20] G. Le Breton and L. Joly, "Molecular modeling of aqueous electrolytes at interfaces: Effects of long-range dispersion forces and of ionic charge rescaling," J. Chem. Phys. **152**(24), 241102 (2020).
[21] S. Yadav and A. Chandra, "Preferential solvation, ion pairing, and dynamics of concentrated aqueous solutions of divalent metal nitrate salts," J. Chem. Phys. **147**(24), 244503 (2017).
[22] P. Habibi, A. Rahbari, S. Blazquez, C. Vega, P. Dey, T. J. H. Vlugt, and O. A. Moultos, "A new force field for OH^- for computing thermodynamic and transport properties of H_2 and O_2 in aqueous NaOH and KOH solutions," J. Phys. Chem. B **126**, 9376 (2022).
[23] S. Blazquez, M. de Lucas, C. Vega, J. Troncoso, and F. Gámez, "The temperature of maximum in density of aqueous solutions of nitrate and ammonium salts: Testing the Madrid-2019 force field," J. Chem. Phys. **161**(4), 046103 (2024).
[24] L. F. Sedano, S. Blazquez, E. G. Noya, C. Vega, and J. Troncoso, "Maximum in density of electrolyte solutions: Learning about ion–water interactions and testing the Madrid-2019 force field," J. Chem. Phys. **156**(15), 154502 (2022).
[25] F. Gámez, L. F. Sedano, S. Blazquez, J. Troncoso, and C. Vega, "Building a Hofmeister-like series for the maximum in density temperature of aqueous electrolyte solutions," J. Mol. Liq. **377**, 121433 (2023).
[26] S. Blazquez, J. Troncoso, P. L. Francesca, P. Gallo, M. M. Conde, and C. Vega, "Extending the Madrid-2019 force field to the perchlorate anion: Role of charge distribution and validation with experiments on Mars-relevant aqueous solutions," J. Mol. Liq. **435**, 128035 (2025).
[27] M. de Lucas, S. Blazquez, J. Troncoso, C. Vega, and F. Gámez, "Dressing a non-polarizable force field for OH^- in TIP4P/2005 aqueous solutions with corrected Hirshfeld charges," J. Phys. Chem. Lett. **15**, 9411–9418 (2024).
[28] D. van der Spoel, E. Lindahl, B. Hess, G. Groenhof, A. E. Mark, and H. J. C. Berendsen, "GROMACS: Fast, flexible and free," J. Comput. Chem. **26**, 1701–1718 (2005).
[29] B. Hess, C. Kutzner, D. van der Spoel, and E. Lindahl, "GROMACS 4: Algorithms for highly efficient, load-balanced, and scalable molecular simulation," J. Chem. Theory Comput. **4**, 435–447 (2008).
[30] S. Nosé, "A molecular dynamics method for simulations in the canonical ensemble," Mol. Phys. **52**(2), 255–268 (1984).
[31] W. G. Hoover, "Canonical dynamics: Equilibrium phase-space distributions," Phys. Rev. A **31**, 1695–1697 (1985).
[32] M. Parrinello and A. Rahman, "Polymorphic transitions in single crystals: A new molecular dynamics method," J. Appl. Phys. **52**, 7182–7190 (1981).

[33]D. Beeman, "Some multistep methods for use in molecular dynamics calculations," J. Comput. Phys. **20**(2), 130–139 (1976).
[34]U. Essmann, L. Perera, M. L. Berkowitz, T. Darden, H. Lee, and L. G. Pedersen, "A smooth particle mesh Ewald method," J. Chem. Phys. **103**, 8577–8593 (1995).
[35]S. Blazquez, M. M. Conde, J. L. F. Abascal, and C. Vega, "The Madrid-2019 force field for electrolytes in water using TIP4P/2005 and scaled charges: Extension to the ions F^-, Br^-, I^-, Rb^+, and Cs^+," J. Chem. Phys. **156**(4), 044505 (2022).
[36]A. Goswami, S. Blazquez, L. F. Sedano, E. G. Noya, H. Jonsson, J. Troncoso, and C. Vega, "Viscosity as a smoking gun for complex formation in solution: Fe^{2+} and Mg^{2+} chlorides as examples," J. Phys. Chem. B **130**, 3436 (2026).
[37]J. L. F. Abascal and C. Vega, "A general purpose model for the condensed phases of water: TIP4P/2005," J. Chem. Phys. **123**(23), 234505 (2005).
[38]B. Hess, H. Bekker, H. J. C. Berendsen, and J. G. E. M. Fraaije, "LINCS: A linear constraint solver for molecular simulations," J. Comput. Chem. **18**(12), 1463–1472 (1997).
[39]J. P. Ryckaert, G. Ciccotti, and H. J. C. Berendsen, "Numerical integration of the Cartesian equations of motion of a system with constraints. Molecular dynamics of *n*-alkanes," J. Comput. Phys. **23**, 327–341 (1977).
[40]M. e. Frisch, G. Trucks, H. B. Schlegel, G. Scuseria, M. Robb, J. Cheeseman, G. Scalmani, V. Barone, G. Petersson, H. Nakatsuji *et al.*, Gaussian 16, Gaussian, Inc., 2016.
[41]T. Lu and F. Chen, "Multiwfn: A multifunctional wavefunction analyzer," J. Comput. Chem. **33**(5), 580–592 (2012).
[42]S. V. Sambasivarao and O. Acevedo, "Development of OPLS-AA force field parameters for 68 unique ionic liquids," J. Chem. Theory Comput. **5**(4), 1038–1050 (2009).
[43]B. Doherty, X. Zhong, S. Gathiaka, B. Li, and O. Acevedo, "Revisiting OPLS force field parameters for ionic liquid simulations," J. Chem. Theory Comput. **13**, 6131–6145 (2017).
[44]A. P. de la Luz, J. A. Aguilar-Pineda, J. G. Méndez-Bermúdez, and J. Alejandre, "Force field parametrization from the Hirshfeld molecular electronic density," J. Chem. Theory Comput. **14**, 5949–5958 (2018).
[45]J. Carmona-Espíndola, E. Núñez-Rojas, V. García-Melgarejo, J. L. Gázquez, and J. Alejandre, "Constrained dipole moment density functional theory for charge distributions in force fields for the study of molecular fluids," J. Chem. Phys. **152**(12), 124116 (2020).
[46]T. Lu and F. Chen, "Atomic dipole moment corrected Hirshfeld population method," J. Theory Comput. Chem. **11**(01), 163–183 (2012).
[47]T. Verstraelen, S. Vandenbrande, F. Heidar-Zadeh, L. Vanduyfhuys, V. Van Speybroeck, M. Waroquier, and P. W. Ayers, "Minimal basis iterative stockholder: Atoms in molecules for force-field development," J. Chem. Theory Comput. **12**(8), 3894–3912 (2016).
[48]F. L. Hirshfeld, "Bonded-atom fragments for describing molecular charge densities," Theor. Chim. Acta **44**(2), 129–138 (1977).
[49]C. J. Cramer and D. G. Truhlar, "Implicit solvation models: Equilibria, structure, spectra, and dynamics," J. Comput. Chem. **99**(8), 2161 (1999).
[50]J. Zhang and T. Lu, "Efficient evaluation of electrostatic potential with computerized optimized code," Phys. Chem. Chem. Phys. **23**(36), 20323–20328 (2021).
[51]B. H. Besler, K. M. Merz, Jr., and P. A. Kollman, "Atomic charges derived from semiempirical methods," J. Comput. Chem. **11**(4), 431–439 (1990).
[52]I. C. Yeh and G. Hummer, "System-size dependence of diffusion coefficients and viscosities from molecular dynamics simulations with periodic boundary conditions," J. Phys. Chem. B **108**, 15873–15879 (2004).
[53]M. A. González and J. L. F. Abascal, "The shear viscosity of rigid water models," J. Chem. Phys. **132**(9), 096101 (2010).
[54]M. C. C. Ribeiro and L. C. J. Almeida, "Validating a polarizable model for the glass-forming liquid $Ca_{0.4}K_{0.6}(NO_3)_{1.4}$ by *ab initio* calculations," J. Chem. Phys. **113**, 4722–4731 (2000).
[55]Y. J. Chung and S. W. Rick, "The effects of charge transfer interactions on the properties of ice Ih," J. Stat. Phys. **145**(2), 355–364 (2011).
[56]J. K. Gregory, D. C. Clary, K. Liu, M. G. Brown, and R. J. Saykally, "The water dipole moment in water clusters," Science **275**(5301), 814–817 (1997).
[57]Y. S. Badyal, M.-L. Saboungi, D. L. Price, S. D. Shastri, D. R. Haeffner, and A. K. Soper, "Electron distribution in water," J. Chem. Phys. **112**(21), 9206–9208 (2000).
[58]A. V. Gubskaya and P. G. Kusalik, "The total molecular dipole moment for liquid water," J. Chem. Phys. **117**(11), 5290–5302 (2002).
[59]E. R. Batista, S. S. Xantheas, and H. Jönsson, "Molecular multipole moments of water molecules in ice Ih," J. Chem. Phys. **109**(11), 4546–4551 (1998).
[60]E. R. Batista, S. S. Xantheas, and H. Jönsson, "Multipole moments of water molecules in clusters and ice Ih from first principles calculations," J. Chem. Phys. **111**(13), 6011–6015 (1999).
[61]J. A. Morrone and R. Car, "Nuclear quantum effects in water," Phys. Rev. Lett. **101**(1), 017801 (2008).
[62]M. Sharma, R. Resta, and R. Car, "Dipolar correlations and the dielectric permittivity of water," Phys. Rev. Lett. **98**(24), 247401 (2007).
[63]J. L. F. Abascal and C. Vega, "Dipole-quadrupole force ratios determine the ability of potential models to describe the phase diagram of water," Phys. Rev. Lett. **98**(23), 237801 (2007).
[64]J. L. F. Abascal and C. Vega, "The water forcefield: Importance of dipolar and quadrupolar interactions," J. Phys. Chem. C **111**(43), 15811–15822 (2007).
[65]M. Despretz, "Recherches sur le maximum de densite des dissolutions aqueuses," Ann. Chim. Phys **70**, 49–81 (1839).
[66]M. Despretz, "Le maximum de densite des liquides," Ann. Chim. Phys **73**, 296–310 (1840).
[67]M. Laliberté and W. E. Cooper, "Model for calculating the density of aqueous electrolyte solutions," J. Chem. Eng. Data **49**(5), 1141–1151 (2004).
[68]M. Laliberté, "Model for calculating the viscosity of aqueous solutions," J. Chem. Eng. Data **52**(4), 1507–1508 (2007).
[69]M. Laliberté, "A model for calculating the heat capacity of aqueous solutions, with updated density and viscosity data," J. Chem. Eng. Data **54**, 1725–1760 (2009).
[70]K. Tanaka, "Measurements of self-diffusion coefficients of water in pure water and in aqueous electrolyte solutions," J. Chem. Soc., Faraday Trans. 1 **71**, 1127–1131 (1975).
[71]D. W. McCall and D. C. Douglass, "The effect of ions on the self-diffusion of water. I. Concentration dependence," J. Phys. Chem. **69**(6), 2001 (1965).
[72]Y.-H. Li and S. Gregory, "Diffusion of ions in sea water and in deep-sea sediments," Geochim. Cosmochim. Acta **38**, 703–714 (1974).
[73]Y. Kameda, H. Saitoh, and O. Uemura, "The hydration structure of NO_3^- in concentrated aqueous sodium nitrate solutions," Bull. Chem. Soc. Jpn. **66**, 1919–1923 (1993).
[74]G. W. Neilson and J. E. Enderby, "The structure around nitrate ions in concentrated aqueous solutions," J. Phys. C: Solid State Phys. **15**, 2347–2352 (1982).
[75]J. L. Thomas, M. Roeselová, L. X. Dang, and D. J. Tobias, "Molecular dynamics simulations of the solution–air interface of aqueous sodium nitrate," J. Phys. Chem. A **111**(16), 3091–3098 (2007).
[76]L. X. Dang, T.-M. Chang, M. Roeselova, B. C. Garrett, and D. J. Tobias, "On NO_3^--H_2O interactions in aqueous solutions and at interfaces," J. Chem. Phys. **124**(6), 066101 (2006).
[77]V. Vchirawongkwin, H. Sato, and S. Sakaki, "RISM-SCF-SEDD study on the symmetry breaking of carbonate and nitrate anions in aqueous solution," J. Phys. Chem. B **114**(32), 10513–10519 (2010).
[78]P. Banerjee, S. Yashonath, and B. Bagchi, "Rotation driven translational diffusion of polyatomic ions in water: A novel mechanism for breakdown of Stokes-Einstein relation," J. Chem. Phys. **146**(16), 164502 (2017).
[79]H.-W. Wang, L. Vlcek, J. C. Neuefeind, K. Page, S. Irle, J. M. Simonson, and A. G. Stack, "Decoding oxyanion aqueous solvation structure: A potassium nitrate example at saturation," J. Phys. Chem. B **122**, 7584–7589 (2018).
[80]G. W. Neilson and R. H. Tromp, "Neutron and x-ray diffraction on aqueous solutions," Annu. Rep. Sec. C (Phys. Chem.) **88**, 45 (1991).
[81]J. E. Enderby, "Ion solvation via neutron scattering," Chem. Soc. Rev. **24**, 159 (1995).

[82]G. W. Neilson and J. E. Enderby, "Aqueous solutions and neutron scattering," J. Phys. Chem. **100**, 1317 (1996).
[83]A. A. Chialvo and L. Vlcek, "NO_3^- – coordination in aqueous solutions by $^{15}N/^{14}N$ and $^{18}O/^{nat}O$ isotopic substitution: What can we learn from molecular simulation?," J. Phys. Chem. B **119**, 519 (2015).
[84]L. F. Sedano, L. C. Pardo, G. Madrigal, E. G. Noya, and C. Vega, "Structure making and breaking in electrolyte solutions explained by water energetics," Proc. Natl. Acad. Sci. U. S. A. **123**, e2531352123 (2026).
[85]D. Biriukov, H.-W. Wang, N. Rampal, C. Tempra, P. Kula, J. C. Neuefeind, A. G. Stack, and M. Předota, "The 'good,' the 'bad,' and the 'hidden' in neutron scattering and molecular dynamics of ionic aqueous solutions," J. Chem. Phys. **156**(19), 194505 (2022).
[86]A. Chattopadhyay, V. Mandalaparthy, and N. F. A. van der Vegt, "Determination of aqueous solubility of nacl in molecular dynamics simulation using the Kirkwood–Buff method," J. Chem. Phys. **162**(17), 174116 (2025).
[87]J. L. F. Abascal, E. Sanz, R. G. Fernandez, and C. Vega, "A potential model for the study of ices and amorphous water: TIP4P/Ice," J. Chem. Phys. **122**(23), 234511 (2005).
[88]S. Blazquez, L. F. Sedano, and C. Vega, "On the compatibility of the Madrid-2019 force field for electrolytes with the TIP4P/Ice water model," J. Chem. Phys. **161**(22), 224502 (2024).
[89]A. Omranpour, P. Montero De Hijes, J. Behler, and C. Dellago, "Perspective: Atomistic simulations of water and aqueous systems with machine learning potentials," J. Chem. Phys. **160**(17), 170901 (2024).